

IDŐJÁRÁS

*Quarterly Journal of the Hungarian Meteorological Service
Vol. 111, No. 1, January–March 2007, pp. 1–40*

Greenhouse effect in semi-transparent planetary atmospheres

Ferenc M. Miskolczi

*Holston Lane 3, Hampton VA 23664, U.S.A.
E-mail: fmiskolczi@cox.net*

(Manuscript received in final form October 29, 2006)

Abstract—In this work the theoretical relationship between the clear-sky outgoing infrared radiation and the surface upward radiative flux is explored by using a realistic finite semi-transparent atmospheric model. We show that the fundamental relationship between the optical depth and source function contains real boundary condition parameters. We also show that the radiative equilibrium is controlled by a special atmospheric transfer function and requires the continuity of the temperature at the ground surface. The long standing misinterpretation of the classic semi-infinite Eddington solution has been resolved. Compared to the semi-infinite model, the finite semi-transparent model predicts much smaller ground surface temperature and a larger surface air temperature. The new equation proves that the classic solution significantly overestimates the sensitivity of greenhouse forcing to optical depth perturbations. In Earth-type atmospheres sustained planetary greenhouse effect with a stable ground surface temperature can only exist at a particular planetary average flux optical depth of 1.841. Simulation results show that the Earth maintains a controlled greenhouse effect with a global average optical depth kept close to this critical value. The broadband radiative transfer in the clear Martian atmosphere follows different principle resulting in different analytical relationships among the fluxes. Applying the virial theorem to the radiative balance equation, we present a coherent picture of the planetary greenhouse effect.

Key-words: greenhouse effect, radiative equilibrium.

1. Introduction

Recently, using powerful computers, virtually any atmospheric radiative transfer problem can be solved by numerical methods with the desired accuracy without using extensive approximations and complicated mathematical expressions common in the literature of the theoretical radiative transfer. However, to improve the understanding of the radiative transfer processes, it is sometimes

useful to apply reasonable approximations and to arrive at solutions in more or less closed mathematical forms which clearly reflect the physics of the problem.

Regarding the planetary greenhouse effect, one must relate the amount of the atmospheric infrared (IR) absorbers to the surface temperature and the total absorbed short wave (SW) radiation. In this paper we derive purely theoretical relationships between the above quantities by using a simplified one dimensional atmospheric radiative transfer model. The relationships among the broadband atmospheric IR fluxes at the boundaries are based on the flux optical depth. The atmospheric total IR flux optical depths are obtained from sophisticated high-resolution spectral radiative transfer computations.

2. Radiative transfer model

In *Fig. 1* our semi-transparent clear sky planetary atmospheric model and the relevant (global mean) radiative flux terms are presented.

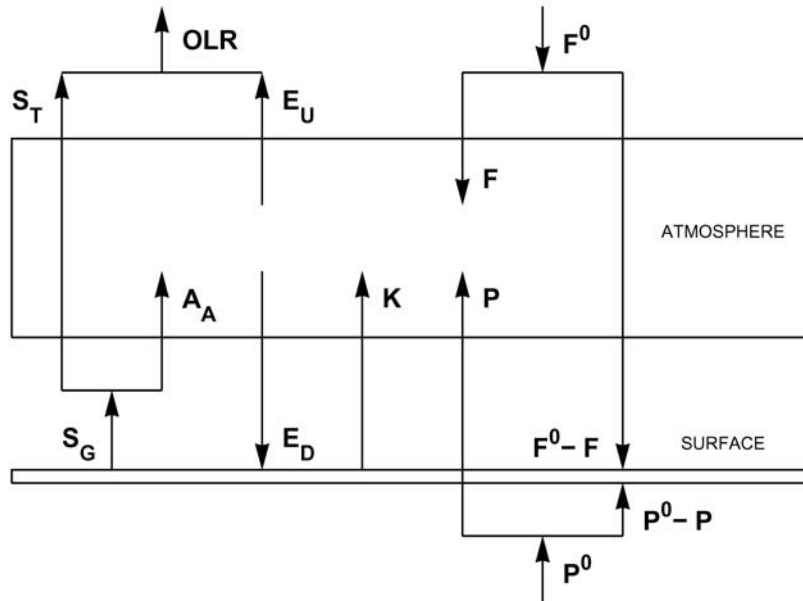


Fig. 1. Radiative flux components in a semi-transparent clear planetary atmosphere. Short wave downward: F^0 and F ; long wave downward: E_D ; long wave upward: OLR , E_U , S_T , A_A , and S_G ; non-radiative origin: K , P^0 and P .

Here F^0 is the total absorbed SW radiation in the system, F is the part of F^0 absorbed within the atmosphere, E_D is the long wave (LW) downward atmospheric radiation, OLR is the outgoing LW radiation, E_U is the LW upward atmospheric radiation. S_G is the LW upward radiation from the ground: $S_G = \sigma t_G^4$, where t_G is the ground temperature and σ is the Stefan-Boltzmann constant. S_T and A_A are the transmitted and absorbed parts of S_G , respectively.

The total thermal energy from the planetary interior to the surface-atmosphere system is P^0 . P is the absorbed part of P^0 in the atmosphere. The net thermal energy to the atmosphere of non-radiative origin is K . The usual measure of the clear-sky atmospheric greenhouse effect is the $G = S_G - OLR$ greenhouse factor (*Inamdar and Ramanathan, 1997*). The normalized greenhouse factor is defined as the $G_N = G/S_G$ ratio. In some work the S_G/OLR ratio is also used as greenhouse parameter (*Stephens et al., 1993*).

Our model assumptions are quite simple and general:

(a) — The available SW flux is totally absorbed in the system. In the process of thermalization F^0 is instantly converted to isotropic upward and downward LW radiation. The absorption of the SW photons and emission of the LW radiation are based on independent microphysical processes.

(b) — The temperature or source function profile is the result of the equilibrium between the IR radiation field and all other sinks and sources of thermal energy (latent heat transfer, convection, conduction, advection, turbulent mixing, short wave absorption, etc.). Note, that the K term is not restricted to strict vertical heat transfer. Due to the permanent motion of the atmosphere K represents a statistical or climatic average.

(c) — The atmosphere is in local thermodynamic equilibrium (LTE). In case of the Earth this is true up to about 60 km altitude.

(d) — The surface heat capacity is equal to zero, the surface emissivity ε_G is equal to one, and the surface radiates as a perfect blackbody.

(e) — The atmospheric IR absorption and emission are due to the molecular absorption of IR active gases. On the Earth these gases are minor atmospheric constituents. On the Mars and Venus they are the major components of the atmosphere.

(f) — In case of the Earth it is also assumed that the global average thermal flux from the planetary interior to the surface-atmosphere system is negligible, $P^0 = 0$. The estimated geothermal flux at the surface is less than 0.03 per cent of F^0 (*Peixoto and Oort, 1992*). However, in our definition P^0 is not restricted to the geothermal flux. It may contain the thermal energy released into the atmosphere by volcanism, tidal friction, or by other natural and non-natural sources.

(g) — The atmosphere is a gravitationally bounded system and constrained by the virial theorem: the total kinetic energy of the system must be half of the total gravitational potential energy. The surface air temperature, t_A , is linked to the total gravitational potential energy through the surface pressure and air density. The temperature, pressure, and air density obey the gas law, therefore, in terms of radiative flux $S_A = \sigma t_A^4$ represents also the total gravitational potential energy.

(h) — In the definition of the greenhouse temperature change keeping t_A and t_G different could pose some difficulties. Since the air is in permanent physical contact with the surface, it is reasonable to assume that, in the average sense, the surface and close-to-surface air are in thermal equilibrium: $t_S = t_A = t_G$, where t_S is the equilibrium temperature. The corresponding equilibrium blackbody radiation is $S_U = \sigma t_S^4$. For now, in *Fig. 1* S_G is assumed to be equal to S_U .

Assumptions (c), (d), (e), and (f) are commonly applied in broadband LW flux computations, see for example in *Kiehl and Trenberth (1997)*. Under such conditions the energy balance equation of the atmosphere may be written as:

$$F + P + K + A_A - E_D - E_U = 0. \quad (1)$$

The balance equation at the lower boundary (surface) is:

$$F^0 + P^0 + E_D - F - P - K - A_A - S_T = 0. \quad (2)$$

The sum of these two equations results in the general relationship of:

$$F^0 + P^0 = S_T + E_U = OLR. \quad (3)$$

This is a simple radiative (energy) balance equation and not related to the vertical structure of the atmosphere. For the Earth this equation simplifies to the well known relationship of $F^0 = OLR$. For long term global mean fluxes these balance equations are exact and they are the requirements for the steady-state climate. However, they do not necessarily hold for zonal or regional averages or for instantaneous local fluxes.

The most apparent reason of any zonal or local imbalance is related to the K term through the general circulation. For example, evaporation and precipitation must be balanced globally, but due to transport processes, they can add or remove optical depth to and from an individual air column in a non-balanced way. The zonal and meridional transfer of the sensible heat is another example.

When comparing clear sky simulation results of the LW fluxes, one should be careful with the cloud effects. Due to the SW effect of the cloud cover on F^0 and F , clear sky computations based on all sky radiosonde observations will also introduce deviations from the balance equations.

The true all sky outgoing LW radiation, OLR^A , must be computed from the clear OLR and the cloudy OLR^C fluxes as the weighted average by the fractional cloud cover: $OLR^A = (1 - \beta)OLR + \beta OLRC$, where β is the fractional cloud cover. Because of the large variety of cloud types and cloud cover and the required additional information on the cloud top altitude, temperature, and emissivity, the simulation of OLR^C is rather complicated.

The global average OLR^A may be estimated from the bolometric planetary equilibrium temperature. From the *ERBE* (2004) data product we estimated the five year average planetary equilibrium temperature as $t_E = 253.8$ K, which resulted in a global average $OLR^A = 235.2$ W m⁻². From the same data product the global average clear-sky OLR is 266.4 W m⁻².

3. Kirchhoff law

According to the Kirchhoff law, two systems in thermal equilibrium exchange energy by absorption and emission in equal amounts, therefore, the thermal energy of either system can not be changed. In case the atmosphere is in thermal equilibrium with the surface, we may write that:

$$A_A = S_U A = S_U (1 - T_A) = E_D. \quad (4)$$

By definition the atmospheric flux transmittance T_A is equal to the S_T / S_U ratio: $T_A = 1 - A = \exp(-\tilde{\tau}_A) = S_T / S_U$, where A is the flux absorptance and $\tilde{\tau}_A$ is the total IR flux optical depth. The validity of the Kirchhoff law – concerning the surface and the inhomogeneous atmosphere above – is not trivial. Later, using the energy minimum principle, we shall give a simple theoretical proof of the Kirchhoff law for atmospheres in radiative equilibrium.

In *Fig. 2* we present large scale simulation results of A_A and E_D for two measured diverse planetary atmospheric profile sets. Details of the simulation exercise above were reported in *Miskolczi and Mlynczak (2004)*. This figure is a proof that the Kirchhoff law is in effect in real atmospheres. The direct consequences of the Kirchhoff law are the next two equations:

$$E_U = F + K + P, \quad (5)$$

$$S_U - (F^0 + P^0) = E_D - E_U. \quad (6)$$

The physical interpretations of these two equations may fundamentally change the general concept of greenhouse theories.

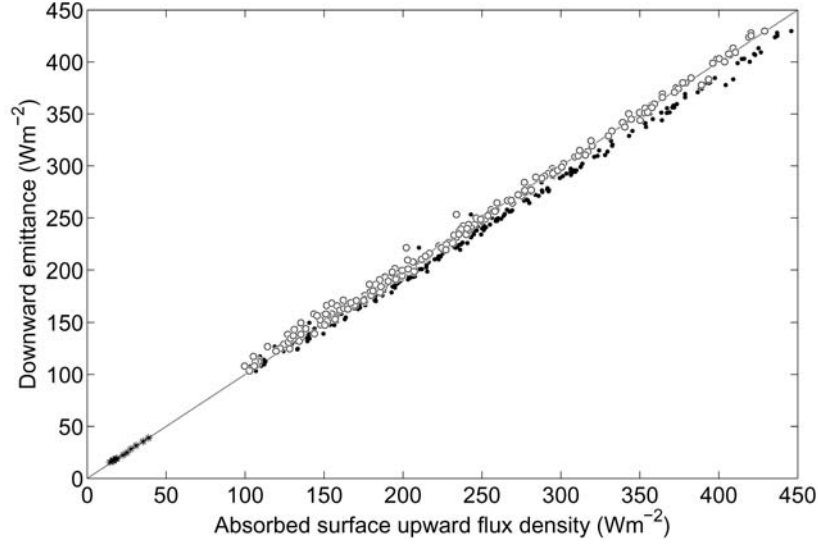


Fig. 2. Simulation results of A_A and E_D . Black dots and open circles represent 228 selected radiosonde observations with $\varepsilon_G = 1$ and $\varepsilon_G = 0.96$, respectively. Black stars are simulation results for Martian standard atmospheric profiles with $\varepsilon_G = 1$. We used two sets of eight standard profiles. One set contained no water vapor and in the other the water vapor concentration was set to constant 210 ppmv (approximately 0.0015 prcm H₂O).

3.1 Upward atmospheric radiation

Eq. (5) shows that the source of the upward atmospheric radiation is not related to LW absorption processes. The $F + K + P$ flux term is always dissipated within the atmosphere increasing (or decreasing) its total thermal energy. The $E_D = S_U - S_T$ functional relationship implies that $G - E_D = -E_U$, therefore, the interpretation of $G - E_D$ as the LW radiative heating (or cooling) of the atmosphere in *Inamdar and Ramanathan (1997)* could be misleading.

Regarding the origin, E_U is more closely related to the total internal kinetic energy of the atmosphere, which – according to the virial theorem – in hydrostatic equilibrium balances the total gravitational potential energy. To identify E_U as the total internal kinetic energy of the atmosphere, the $E_U = S_U / 2$ equation must hold. E_U can also be related to G_N through the $E_U = S_U (A - G_N)$ equation. In opaque atmospheres $A = 1$ and the $G_N = 0.5$ is the theoretical upper limit of the normalized greenhouse factor.

3.2 Hydrostatic equilibrium

In Eq. (6) $S_U - (F^0 + P^0)$ and $E_D - E_U$ represent two flux terms of equal magnitude, propagating into opposite directions, while using the same F^0 and P^0 as energy sources. The first term heats the atmosphere and the second term maintains the surface energy balance. The principle of conservation of energy dictates that:

$$S_U - (F^0 + P^0) + E_D - E_U = F^0 + P^0 = OLR. \quad (7)$$

This equation poses a strict criterion on the global average S_U :

$$S_U = 3OLR/2 \rightarrow S_U - (F^0 + P^0) = R. \quad (8)$$

In the right equation R is the pressure of the thermal radiation at the ground: $R = S_U/3$. This equation might make the impression that G does not depend on the atmospheric absorption, which is generally not true. We shall see that under special conditions this dependence is negligible. Eq. (8) expresses the conservation of radiant energy but does not account for the fact, that the atmosphere is gravitationally bounded. Implementing the virial theorem into Eq. (8) is relatively simple. In the form of an additive S_V ‘virial’ term we obtained the general radiative balance equation:

$$S_U + S_T/2 - E_D/10 = 3OLR/2 \rightarrow S_U - (F^0 + P^0) = 6RA/5. \quad (9)$$

In Eq. (9) the $S_V = S_T/2 - E_D/10$ virial term will force the hydrostatic equilibrium while maintaining the radiative balance. From Eq. (9) follow the $3/5 + 2T_A/5 = OLR/S_U$ and the $E_U/E_D = 3/5$ relations. This equation is based on the principle of the conservation of energy and the virial theorem, and we expect that it will hold for any clear absorbing planetary atmosphere.

The optimal conversion of $F^0 + P^0$ to OLR would require that either $T_A \approx 0$ or $T_A \approx 1$. The first case is a planet with a completely opaque atmosphere with saturated greenhouse effect, and the second case is a planet without greenhouse gases. For the Earth obviously the $T_A \approx 0$ condition apply and the $OLR^A/S_U^A = 3/5$ equation gives an optimal global average surface upward flux of $S_U^A = 392 \text{ W m}^{-2}$ and a global average surface temperature of 288.3 K. We know that – because of the existence of the IR atmospheric window – the flux transmittance must not be zero and the atmosphere can not be opaque. The Earth’s atmosphere solves this contradiction by using the radiative effect of a partial cloud cover.

For atmospheres, where $E_D \approx 5S_T$ or $T_A \approx 1/6$, Eq. (9) will take the form of Eq. (8). In optically thin atmospheres where, $E_D/10 \ll OLR$ or $S_T \gg E_U$, Eq. (9) simplifies to:

$$S_U + S_T/2 = 3OLR/2 \rightarrow S_U - (F^0 + P^0) = RA. \quad (10)$$

Eq. (10) implies the $2/3 + T_A/3 = OLR/S_U$ and $E_U/E_D = 2/3$ relations. Applying this equation for the Earth's atmosphere will introduce more than 10% error in the OLR .

3.2 Transfer and greenhouse functions

The relationships between the OLR and S_U may be expressed by using the concept of the transfer function. The transfer function converts the surface upward radiation to outgoing LW radiation. It is practically the OLR/S_U ratio or the normalized OLR . The greenhouse functions are analogous to the empirical G_N factor introduced in Section 2. From Eqs. (8), (9), and (10) one may easily derive the $f^+ = 2/3$, $f^\circ = 1 - 2A/5$, and $f^* = 1 - A/3$ transfer functions, and the $g^+ = 1/3$, $g^\circ = 2A/5$, and $g^* = A/3$ greenhouse functions, respectively. The g^+ , g° , and g^* greenhouse functions will always satisfy the $S_U > F^0 + P^0$ relationship, which is the basic requirement of the greenhouse effect. On the evolutionary time scale of a planet, the mass and the composition of the atmosphere together with the F^0 and P^0 fluxes may change dramatically and accordingly, the relevant radiative balance equation could change with the time and could be different for different planets.

The most interesting fact is, that in case of Eq. (8) $g^+ = R/S_U = 1/3$ does not depend on the optical depth. G will always be equal to the radiation pressure of the ideal gas, and the atmosphere will have a constant optical depth $\tilde{\tau}_A^+$ which is only dependent on the sum of the external SW and internal thermal radiative forcings. In Eqs. (9) and (10) the dependence of G on A is expected. Planets following the radiation scheme of Eq. (8) can not change their surface temperature without changing the surface pressure – total mass of the atmosphere – or the SW or thermal energy input to the system. This kind of planet should have relatively strong absorption ($T_A \approx 1/6$), and the greenhouse gases must be the minor atmospheric constituents with very small effect on the surface pressure. Earth is a planet of this kind. In the Martian atmosphere E_U is far too small and in the Venusian atmosphere S_G is far too large to satisfy the $E_U \approx S_U/2$ condition, moreover, the atmospheric absorption on these planets significantly changes with the mass of the atmosphere – or with the surface pressure.

Our simulations show that on the Earth the global average transmitted radiative flux and downward atmospheric radiation are $S_T^E = 61 \text{ W m}^{-2}$ and $E_D^E = 309 \text{ W m}^{-2}$. The $S_T^E \approx E_D^E/5$ approximation holds and Eq. (8) with the g^+ greenhouse function may be used. The global average clear sky S_U and OLR

are $S_U^E = 382 \text{ W m}^{-2}$ and $OLR^E = 250 \text{ W m}^{-2}$. Correcting this S_U^E to the altitude level where the OLR was computed (61.2 km), we may calculate the global average G_N as $G_N^E = (S_U^E - OLR^E) / S_U^E = 0.332$. In fact, G_N^E is in very good agreement with the theoretical $g^+ = 0.333$. The simulated global average flux optical depth is $\tilde{\tau}_A^E = -\ln(T_A^E) = 1.87$, where T_A^E is the global average flux transmittance. This simulated $\tilde{\tau}_A^E$ can not be compared with theoretical optical depths from Eq. (8) without the explicit knowledge of the $S_U(OLR, \tilde{\tau}_A)$ function. The best we can do is to use Eq. (9) – the $T_A = 1/6$ condition – to get an estimate of $\tilde{\tau}_A^+ \approx -\ln(1/6) = 1.79$, which is not very far from our $\tilde{\tau}_A^E$.

The popular explanation of the greenhouse effect as the result of the LW atmospheric absorption of the surface radiation and the surface heating by the atmospheric downward radiation is incorrect, since the involved flux terms (A_A and E_D) are always equal. The mechanism of the greenhouse effect may better be explained as the ability of a gravitationally bounded atmosphere to convert $F^0 + P^0$ to OLR in such a way that the equilibrium source function profile will assure the radiative balance ($F^0 + P^0 = OLR$), the validity of the Kirchhoff law ($E_D = S_U A$), and the hydrostatic equilibrium ($S_U = 2E_U$). Although an atmosphere may accommodate the thermal structure needed for the radiative equilibrium, it is not required for the greenhouse effect. Formally, in the presence of a solid or liquid surface, the radiation pressure of the thermalized photons is the real cause of the greenhouse effect, and its origin is related to the principle of the conservation of the momentum of the radiation field.

Long term balance between $F^0 + P^0$ and OLR can only exist at the $S_U = (F^0 + P^0) / (1 - 2A/5) \approx 3(F^0 + P^0) / 2$ planetary equilibrium surface upward radiation. It worth to note that S_U does not depend directly on F , meaning that the SW absorption may happen anywhere in the system. F^0 depends only on the system albedo, the solar constant, and other relevant astronomical parameters.

In the broad sense the surface-atmosphere system is in the state of radiative balance if the radiative flux components satisfy Eqs. (3), (4), and (8). The equivalent forms of these conditions are the $E_D - E_U = S_U / 3$ and $E_D - E_U = OLR / 2$ equations. In such case there is no horizontal exchange of energy with the surrounding environment, and the use of a one dimensional or single-column model for global energy budget studies is justified.

Our task is to establish the theoretical relationship between S_U and OLR as the function of $\tilde{\tau}_A$ for semi-transparent bounded atmospheres assuming, that the radiative balance (Eqs. (8) and (9)) is maintained and the thermal structure (source function profile) satisfies the criterion of the radiative equilibrium. The evaluation of the response of an atmosphere for greenhouse gas perturbations is only possible with the explicit knowledge of such relationship.

4. Flux optical depth

To relate the total IR absorber amount to the flux densities, the most suitable parameter is the total IR flux optical depth. In the historical development of the gray approximation different spectrally averaged mean optical depths were introduced to deal with the different astrophysical problems (*Sagan, 1969*). If we are interested in the thermal emission, our relevant mean optical depth will be the Planck mean. Unfortunately, the Planck mean works only with very small monochromatic optical depths (*Collins, 2003*). In the Earth atmosphere the infrared monochromatic optical depth is varying many orders of magnitude, therefore, the required criteria for the application of the Planck mean is not satisfied.

This problem can be eliminated without sacrificing accuracy by using the simulated flux optical depth. Such optical depths may be computed from monochromatic directional transmittance by integrating over the hemisphere. We tuned our line-by-line (LBL) radiative transfer code (HARTCODE) for an extreme numerical accuracy, and we were able to compute the flux optical depth in a spherical refractive environment with an accuracy of five significant digits (*Miskolczi et al., 1990*). To obtain this accuracy 9 streams, 150 homogeneous vertical layers, and 1 cm^{-1} spectral resolution were applied. These criteria control the accuracy of the numerical hemispheric and altitude integration and the convolution integral with the blackbody function, see Appendix A.

All over this paper the simulated total flux optical depths were computed as the negative natural logarithms of these high accuracy Planck weighted hemispheric monochromatic transmittance: $\tilde{\tau}_A = -\ln(T_A)$.

In a non-scattering atmosphere, theoretically, the dependence of the source function on the monochromatic optical depth is the solution of the following differential equation (*Goody and Young, 1989*):

$$\frac{d^2 H_\nu(\tau_\nu)}{d\tau_\nu^2} - 3H_\nu(\tau_\nu) = -4\pi \frac{dJ_\nu(\tau_\nu)}{d\tau_\nu}, \quad (11)$$

where $H_\nu(\tau_\nu)$ is the monochromatic net radiative flux (Eddington flux) and $J_\nu(\tau_\nu)$ is the monochromatic source function, which is – in LTE – identical with the Planck function, $J_\nu(\tau_\nu) = B_\nu(\tau_\nu)$. The vertically measured monochromatic optical depth is τ_ν . Eq. (11) assumes the isotropy of the radiation field in each hemisphere and the validity of the Eddington approximation.

For monochromatic radiative equilibrium $dH_\nu(\tau_\nu)/d\tau_\nu = 0$ and Eq. (11) becomes a first order linear differential equation for $B_\nu(\tau_\nu)$. Applying the gray approximation, one finds that there will be no dependence on the wave number, τ_ν will become a mean vertical gray-body optical depth, $\bar{\tau}$, and H will become the net radiative flux:

$$dB(\bar{\tau})/d\bar{\tau} = 3H/(4\pi). \quad (12)$$

The well known solution of Eq. (12) is:

$$B(\bar{\tau}) = (3/4\pi)H\bar{\tau} + B_0. \quad (13)$$

According to Eq. (13), in radiative equilibrium the source function increases linearly with the gray-body optical depth. The integration constant, B_0 , can be determined from the Schwarzschild-Milne equation, which relates the net flux to the differences in the hemispheric mean intensities:

$$H(\bar{\tau}) = \pi(\bar{I}^+ - \bar{I}^-), \quad (14)$$

where \bar{I}^+ and \bar{I}^- are the upward and downward hemispheric mean intensities, respectively. In the solution of Eq. (12) one has to apply the appropriate boundary conditions. In the further discussion we shall allow S_G and S_A to be different.

4.1 Semi-infinite atmosphere

In the semi-infinite atmosphere, the total vertical optical depth of the atmosphere is infinite. The boundary condition is usually given at the top of the atmosphere, where, due to the absence of the downward flux term, the net IR flux is known. Using the general classic solutions of the plane-parallel radiative transfer equation in Eq. (14), one sees that the integration constant will become $B_0 = H/(2\pi)$. Putting this B_0 into Eq. (13) will generate the classic semi-infinite solution for the $B(\bar{\tau})$ source function:

$$B(\bar{\tau}) = H(1 + \bar{\tau})/(2\pi), \quad (15)$$

where $\tilde{\tau}$ is the flux optical depth, as usually defined in two stream approximations, $\tilde{\tau} = (3/2)\bar{\tau}$. In astrophysics monographs Eq. (15) is referred to as the solution of the Schwarzschild-Milne type equation for the gray atmosphere using the Eddington approximation.

The characteristic gray-body optical depth, $\hat{\tau}_C$, defines the IR optical surface of the atmosphere: $\pi B(\hat{\tau}_C) = H$. The ‘hat’ indicates that this is a theoretically computed quantity. At the upper boundary, $\tilde{\tau} = 0$, the source function is finite, and is usually associated with the atmospheric skin temperature: $\pi B_0 = \pi B(0) = H/2$. Note, that in obtaining B_0 , the fact of the semi-infinite integration domain over the optical depth in the formal solution is widely used. For finite or optically thin atmosphere Eq. (15) is not valid. In

other words, this equation does not contain the necessary boundary condition parameters for the finite atmosphere problem.

Despite the above fact, in the literature of atmospheric radiation and greenhouse effect, Eq. (15) is almost exclusively applied to derive the dependence of the surface air temperature and the ground temperature on the total flux optical depth (*Goody and Yung, 1989; Stephens and Greenwald, 1991; McKay et al., 1999; Lorenz and McKay, 2003*):

$$t_A^4 = t_E^4(1 + \tilde{\tau}_A)/2, \quad (16)$$

$$t_G^4 = t_E^4(2 + \tilde{\tau}_A)/2, \quad (17)$$

where $t_A^4 = \pi B(\tilde{\tau}_A)/\sigma$, $t_G^4 = t_A^4 + t_E^4/2$, and $t_E^4 = H/\sigma = OLR/\sigma$ are the surface air temperature, ground temperature, and the effective temperature, respectively. At the top of the atmosphere the net IR radiative flux is equal to the global average outgoing long wave radiation. As we have already seen, when long term global radiative balance exists between the SW and LW radiation, *OLR* is equal to the sum of the global averages of the available SW solar flux and the heat flux from the planetary interior.

Eq. (15) assumes that at the lower boundary the total flux optical depth is infinite. Therefore, in cases, where a significant amount of surface transmitted radiative flux is present in the *OLR*, Eqs. (16) and (17) are inherently incorrect. In stellar atmospheres, where, within a relatively short distance from the surface of a star the optical depth grows tremendously, this could be a reasonable assumption, and Eq. (15) has great practical value in astrophysical applications. The semi-infinite solution is useful, because there is no need to specify any explicit lower boundary temperature or radiative flux parameter (*Eddington, 1916*).

When considering the clear-sky greenhouse effect in the Earth's atmosphere or in optically thin planetary atmospheres, Eq. (16) is physically meaningless, since we know that the *OLR* is dependent on the surface temperature, which conflicts with the semi-infinite assumption that $\tilde{\tau}_A = \infty$. Eq. (17) is also not a prescribed mathematical necessity, but an incorrect assumption for the downward atmospheric radiation and applying the relationship of Eq. (16). As a consequence, Eq. (16) will underestimate t_A , and Eq. (17) will largely overestimate t_G (*Miskolczi and Mlynczak, 2004*).

There were several attempts to resolve the above deficiencies by developing simple semi-empirical spectral models, see for example *Weaver and Ramanathan (1995)*, but the fundamental theoretical problem was never resolved. The source of this inconsistency can be traced back to several decades ago, when the semi-infinite solution was first used to solve bounded atmosphere problems. About 80 years ago Milne stated: "Assumption of infinite thickness

involves little or no loss of generality”, and later, in the same paper, he created the concept of a secondary (internal) boundary (*Milne, 1922*). He did not realize that the classic Eddington solution is not the general solution of the bounded atmosphere problem and he did not re-compute the appropriate integration constant. This is the reason why scientists have problems with a mysterious surface temperature discontinuity and unphysical solutions, as in *Lorenz and McKay (2003)*. To accommodate the finite flux optical depth of the atmosphere and the existence of the transmitted radiative flux from the surface, the proper equations must be derived.

4.2 Bounded atmosphere

In the bounded or semi-transparent atmosphere $OLR = E_U + S_T$. In the Earth’s atmosphere, the lower boundary conditions are well defined and explicitly given by t_A , t_G , and $\tilde{\tau}_A$. The surface upward hemispheric mean radiance is $B_G = S_G/\pi = \sigma t_G^4/\pi$. The upper boundary condition at the top of the atmosphere is the zero downward IR radiance.

The complete solution of Eq. (12) requires only one boundary condition. To evaluate B_0 we can use either the top of the atmosphere or the surface boundary conditions since both of them are defined. Applying the boundary conditions in Eq. (14) at $H = H(0)$ and $H = H(\bar{\tau}_A)$ will yield two different equations for B_0 . The traditional way is to solve this as a system of two independent equations for B_0 and B_G as unknowns, and arrive at the semi-infinite solution with a prescribed temperature discontinuity at the ground. In the traditional way, therefore, B_G becomes a constant, which does not represent the true lower boundary condition.

The source of the problem is, that at the lower boundary B_G is treated as an arbitrary parameter. In reality, when considering the Schwarzschild-Milne equation at $H = H(\bar{\tau}_A)$, we must apply a constraint for B_G . In the introduction we showed that this is set by the total energy balance requirement of the system: $OLR = S_G - E_D + E_U$. Using the above condition for solving Eq. (14) at $H = H(\bar{\tau}_A)$ will be equivalent to solving the same equation at $H = H(0)$. For mathematical simplicity now we introduce the atmospheric transfer and greenhouse functions by the following definitions:

$$f(\tilde{\tau}_A) = 2/(1 + \tilde{\tau}_A + \exp(-\tilde{\tau}_A)), \quad (18)$$

and

$$g(\tilde{\tau}_A) = (\tilde{\tau}_A + \exp(-\tilde{\tau}_A) - 1)/(\tilde{\tau}_A + \exp(-\tilde{\tau}_A) + 1). \quad (19)$$

The f and g are special functions and they have some useful mathematical properties: $f = 1 - g$ and $dg/d\tilde{\tau}_A = -df/d\bar{\tau}_A = f^2 A/2$. Later we shall see that

in case of radiative equilibrium, these functions partition the surface upward radiative flux into the OLR and $S_G - OLR$ parts. Using the above notations the derived B_0 takes the form:

$$\pi B_0 = \frac{H}{2A} \left[\frac{2}{f} - \tilde{\tau}_A A \right] - \pi B_G T_A / A. \quad (20)$$

For large $\tilde{\tau}_A$ this B_0 tends to the semi-infinite solution. Combining Eq. (20) with Eq. (13) we obtain the general form of the source function for the bounded atmosphere:

$$\pi B(\tilde{\tau}) = \frac{H}{2A} \left[\frac{2}{f} - (\tilde{\tau} - \tilde{\tau}_A) A \right] - \pi B_G T_A / A. \quad (21)$$

We call Eq. (21) the general greenhouse equation. It gives the fundamental relationship between $\tilde{\tau}$, $\tilde{\tau}_A$, B_G , H , and the IR radiation fluxes, and this is the equation that links the surface temperatures to the column density of absorber. This equation is general in the sense, that it contains the general boundary conditions of the semi-transparent atmosphere, and asymptotically includes the classic semi-infinite solution. For the validity of Eq. (21) the radiative equilibrium condition (Eq. (12)) must hold.

We could not find any references to the above equation in the meteorological literature or in basic astrophysical monographs, however, the importance of this equation is obvious, and its application in modeling the greenhouse effect in planetary atmospheres may have far reaching consequences.

For example, radiative-convective models usually assume that the surface upward convective flux is due to the temperature discontinuity at the surface. The fact, that the new B_0 (skin temperature) changes with the surface temperature and total optical depth, can seriously alter the convective flux estimates of previous radiative-convective model computations. Mathematical details on obtaining Eqs. (20) and (21) are summarized in Appendix B.

At the upper boundary $H = OLR$, and it is immediately clear that for large $\tilde{\tau}_A$ Eq. (21) converges to the semi-infinite case of Eq. (15). It is also clear that the frequently mentioned temperature discontinuity requirement at the surface has been removed by the explicit dependence of $B(\tilde{\tau})$ on B_G . The derivative of this equation is constant and equal to $3H/(4\pi)$, just like in the semi-infinite case, as it should be. According to Eq. (21), the surface air temperature and the characteristic optical depth depend on B_G and $\tilde{\tau}_A$:

$$\pi B(\tilde{\tau}_A) = (OLR / f - \pi B_G T_A) / A, \quad (22)$$

$$\hat{\tau}_C = 1 + \frac{2(1 - \pi B_G / OLR) + \tilde{\tau}_A}{1 - \exp(\tilde{\tau}_A)}. \quad (23)$$

Particularly simple forms of the OLR and E_U may be derived from Eq. (22):

$$OLR = f(S_A A + S_G T_A), \quad (24)$$

$$E_U = f S_A A - g S_G T_A. \quad (25)$$

In Eqs. (24) and (25) $S_A = \pi B(\tilde{\tau}_A) = \sigma t_A^4$. The upward atmospheric radiation clearly depends on the ground temperature and can not be computed without the explicit knowledge of S_G .

5. Temperature discontinuity

Now we shall again assume the thermal equilibrium at the surface: $t_S = t_A = t_G$. Inevitably, because the radiating ground surface is not a perfect blackbody, $S_U = S_A > S_G$, and $S_G = \varepsilon_G \sigma t_G^4 = \varepsilon_G \sigma t_S^4 = \varepsilon_G S_U$. From Eq. (24) one may easily express t_S :

$$t_S^4 = t_E^4 / (1 + T_A(\varepsilon_G - 1)) / f. \quad (26)$$

For high emissivity and opaque areas the following approximations will hold:

$$t_S^4 = t_E^4 / f, \quad (27)$$

$$S_U = OLR / f. \quad (28)$$

The $E_U / S_U = (OLR - S_T) / S_U = f - T_A$ relationship follows from Eq. (28). This function (normalized upward atmospheric radiation) has a sharp maximum at $\tilde{\tau}_A^U = 1.59$. It is worth noting, that in Eq. (26) the dependence of t_S on ε_G opens up a greenhouse feedback channel which might have importance in relatively transparent areas with low emissivity, for example at ice covered polar regions. Also, Eq. (26) must be the preferred equation to study radiative transfer above cloud layers. Assuming the global averages of $\varepsilon_G = 0.95$ and $T_A = 0.17$, Eq. (27) will underestimate t_S by about 0.9 per cent.

So far at the definition of ε_G we ignored the reflected part of the downward long-wave flux. The true surface emissivity is: $\varepsilon'_G = E_D T_A / (S_U - E_D) / A$. ε'_G may be obtained from ε_G by applying the next correction: $\varepsilon'_G = \varepsilon_G T_A / (1 - \varepsilon_G A)$. The energy balance at the boundary is maintained by the net sensible and latent heat

fluxes and other energy transport processes of non-radiative origin. Further on we shall assume that the $\varepsilon_G = \varepsilon'_G = 1$ approximation and Eqs. (27) and (28) are valid. Let us emphasize again, that these equations assume the thermal equilibrium at the ground.

5.1 Energy minimum principle

We may also arrive at Eq. (28) from a rather different route. The principle of minimum energy requires the most efficient disposal of the thermal energy of the atmosphere. Since in radiative equilibrium the quantity πB_0 is an additive constant to the source function, for a given OLR and S_G we may assume that in the atmosphere the total absorber amount (water vapor) will maximize B_0 .

Mathematically, $\tilde{\tau}_A$ is set by the $dB_0/d\tilde{\tau}_A = 0$ condition. It can be shown that this is equivalent to solve the $S_G = OLR/f$ transcendental equation for $\tilde{\tau}_A$, see the details in Appendix B. Comparing this equation with Eq. (28) follows the $S_G = S_U$ equation.

In other words, in radiative equilibrium there is a thermal equilibrium at the ground and the quantities S_G , OLR , and $\tilde{\tau}_A$ are linked together in such a way that $\tilde{\tau}_A$ will maximize B_0 . The above concept is presented in *Fig. 3*. Here we show three πB_0 functions, with short vertical lines indicating the positions of their maxima. The thick solid curve was computed from Eq. (20) with the clear sky global averages of $OLR = 250 \text{ W m}^{-2}$ and $\pi B_G = 382 \text{ W m}^{-2}$. The open circle at $\tilde{\tau}_A = 1.87$ represents the global average πB_0 of 228 simulations.

The position of the maximum of this curve is practically coincidental with the global average $\tilde{\tau}_A^E$. The location of the maximum may be used in a parameterized $H_2O(\tilde{\tau}_A)$ function for the purely theoretical estimate of the global average water vapor content. In such estimate our global average $\tilde{\tau}_A$ would result in about 2.61 precipitable centimeter (prcm) H_2O column amount.

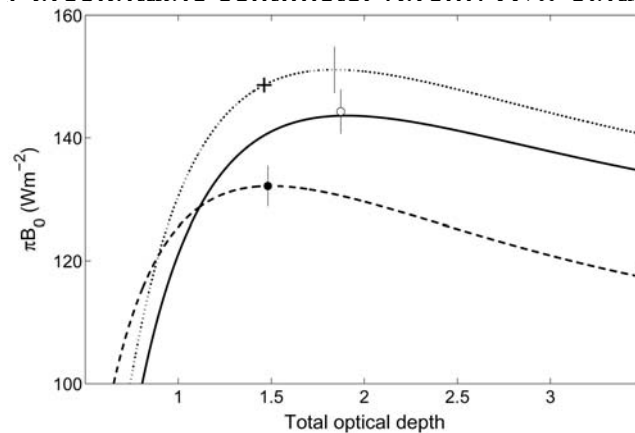


Fig. 3. $\pi B_0(\tilde{\tau}_A)$ functions computed from Eq. (20) for a realistic range of $\tilde{\tau}_A$. The solid line represents the clear-sky global average. The maximum of this curve is $\pi B_0 = 142 \text{ W m}^{-2}$ at $\tilde{\tau}_A = 1.86$. The open circle at $\pi B_0 = 143 \text{ W m}^{-2}$ and $\tilde{\tau}_A = 1.87$ is the global average of large scale line-by-line simulations involving 228 temperature and humidity profiles from around the globe. The broken line and the solid dot were computed for a zonal average arctic profile. The dotted line and the '+' symbol

represent similar computations for the USST-76 atmosphere.

The broken line and the full circle show similar computations for a zonal mean arctic profile. For reference, the $\pi B_0(\tilde{\tau}_A)$ function of the U.S. Standard Atmosphere, 1976 (USST-76) is also plotted with a dotted line. In this case the actual optical depth $\tilde{\tau}_A^{US} = 1.462$ (indicated by the ‘+’ symbol) is not coincidental with the position of the maximum of the $\pi B_0(\tilde{\tau}_A)$ curve, meaning that this profile does not satisfy Eq. (28). Compared to the required equilibrium surface temperature of $t_A^{US} = 280.56$ K, the USST-76 atmosphere is warmer by about 7.6 K at the ground. Some further comparisons of the theoretical and simulated total optical depths are shown in *Fig. 4*.

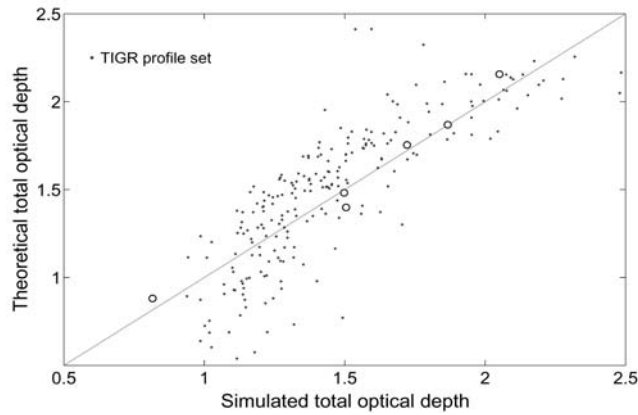


Fig. 4. Comparisons of the theoretical and simulated total flux optical depths. The inner four circles were computed for global and zonal mean temperature profiles, the leftmost circle were computed for an extremely cold arctic profile, the rightmost circle represents a mid-latitude summer profile. The dots show the results of 228 LBL simulations. The scatter of the dots are due to the fact that the temperature profiles were not in perfect radiative equilibrium.

The simulated data points were obtained by LBL computations using zonal mean temperature profiles at different polar and equatorial belts. The theoretical values – the solutions of Eq. (28) – are in fairly good agreement with the simulated $\tilde{\tau}_A$, the correlation coefficient is 0.989. The major conclusion of *Figs. 3* and *4* is the fact that for large scale spatial averages the finite atmosphere problem may be handled correctly with the different forms of Eqs. (24) or (28). For local or instantaneous fluxes (represented by the gray dots) the new equations do not apply because the chances to find an air column in radiative balance are slim.

5.2 Global average profiles

In Fig. 5 we present our global average source function profile – which was computed from selected all-sky radiosonde observations – and the theoretical predictions of the semi-infinite and semi-transparent approximations.

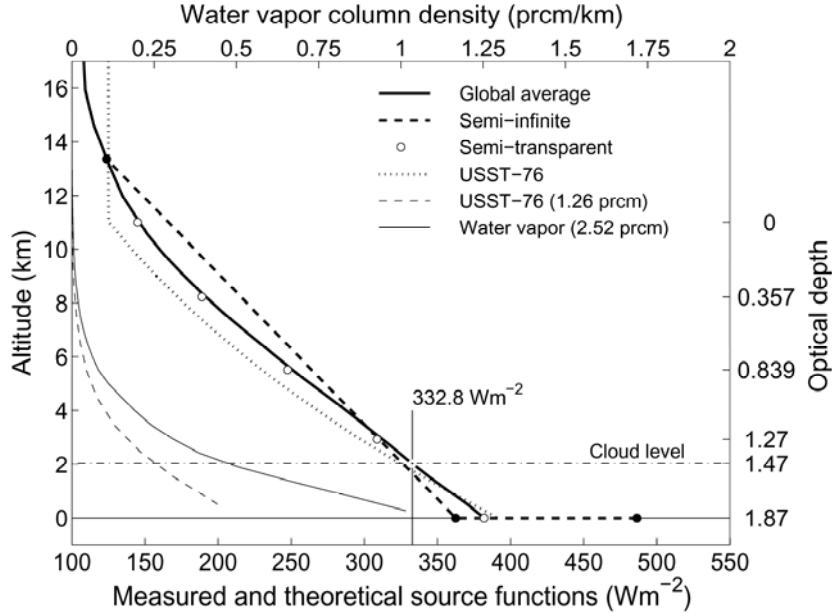


Fig. 5. Theoretical and measured source function profiles, and the global average H_2O profile. The solid lines were computed from 228 selected all sky radiosonde observations. The black dots and the dashed line represent the semi-infinite approximation with the temperature discontinuity at the ground. The open circles were computed from Eq. (21). The optical depth values of 0.357, 0.839, 1.28, 1.47, and 1.87 correspond to $\hat{\tau}_{E_U}$, $\hat{\tau}_C$, $\hat{\tau}_{E_D}$, $\tilde{\tau}_A^C \approx \tilde{\tau}_A^{US}$, and $\tilde{\tau}_A^E$, respectively. The dash-dot line is the approximate altitude of an assumed cloud layer where the $OLR^A = E_D = OLR$.

The source function profile of the USST-76 model atmosphere is also plotted with a dotted line. The global average tropospheric source function profile is apparently a radiative equilibrium profile satisfying Eq. (21) or the $B(\tilde{\tau}) = OLR \tilde{\tau}/2 + B_0$ equation, where $B_0 = 146 \text{ W m}^{-2}$. Up to 10 km altitude the $B(z) \approx OLR^A (1 - z/10) + B_0$ approximation may be used, where the global average OLR^A is: $OLR^A \approx OLR \tilde{\tau}_A^E / 2$.

Clearly the new equations give a far better representation of the true average tropospheric source function profile than the one obtained from the opaque semi-infinite equation. Our source function profile corresponds to a temperature profile with an average tropospheric lapse rate of 5.41 K km^{-1} . The flux densities S_U^E and OLR^E with $\tilde{\tau}_A^E$ closely satisfy Eqs. (8), (9), and (28). This optical depth is consistent with the observed global average water vapor column amount of about 2.5 prcm in Peixoto and Oort (1992).

In *Fig. 5* the thin solid and broken lines – and the top axis – show the water vapor column density profiles of our global average and the USST-76 atmospheres respectively.

Since the Earth-atmosphere system must have a way to reduce the clear sky OLR^E to the observed OLR^A we assume the existence of an effective cloud layer at about 2.05 km altitude. The corresponding optical depth is $\tilde{\tau}_A^C = 1.47$. *Fig. 6* shows the dependences of the OLR and E_D on the cloud top altitude and E_U on the cloud bottom altitude. At this cloud level the source function is $S^C = 332.8 \text{ W m}^{-2}$. We also assume that the cloud layer is in thermal equilibrium with the surrounding air and radiates as a perfect black-body. Clear sky simulations show that at this level the $OLR \approx OLR^A \approx E_D$ and the layer is close to the radiative equilibrium. Cloudy computations also show that E_U – and consequently K – has a maximum around this level, which is favorable for cloud formation.

In cloudy areas the system loses the thermal energy to space at a rate of OLR^A which is now covered by the absorbed SW flux in the cloudy atmosphere. According to the Kirchhoff law, the downward radiation to the cloud top is also balanced. Below the cloud layer, the net LW flux is close to zero. Clouds at around 2 km altitude have minimal effect on the LW energy balance, and they seem to regulate the SW absorption of the system by adjusting the effective cloud cover β .

The $OLR^A - 2S_U^E/3 \approx -15 \text{ W m}^{-2}$ is a fairly good estimate of the global average cloud forcing. The estimated $\beta \approx 0.6$ is the required cloud cover (at this level) to balance OLR^A , which looks realistic. We believe that the β parameter is governed by the maximum entropy principle, the system tries to convert as much SW radiation to LW radiation as possible, while obeying the $2OLR/(3f) = F^0 + P^0$ condition. The cloud altitude, where the clear-sky $OLR = OLR^A = E_D$ depends only on the SW characteristics of the system (surface and cloud albedo, SW solar input) and alone, is a very important climate parameter.

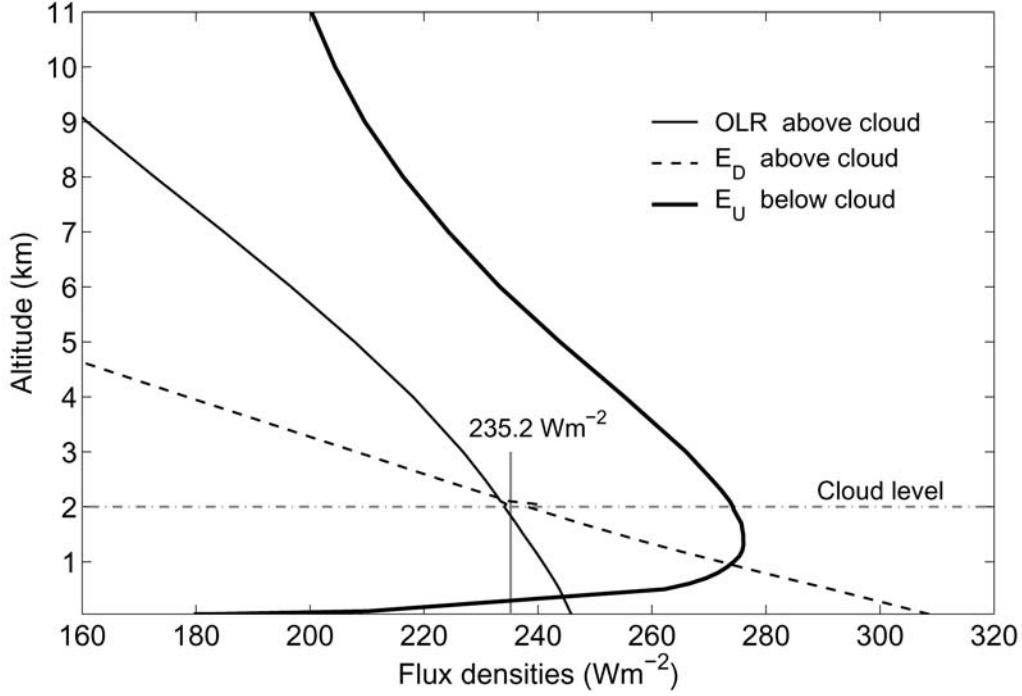


Fig. 6. Cloudy simulation results using the global average temperature and water vapor profiles. For the OLR and E_D curves the altitude is the cloud-top level. For the E_U curve the altitude is the level of the cloud-bottom. Simulations were performed at eleven cloud levels between the 0 and 11 km altitudes. The gray vertical line is the all-sky OLR^A .

In Kiehl and Trenberth (1997) the USST-76 atmosphere was used for the estimation of the clear-sky global mean E_D and OLR . To make their computed OLR consistent with the ERBE clear-sky observations, they reduced the tropospheric water vapor amount by 12%, to about 1.26 prcm. Our LBL simulation using the same profile indicates that $\tilde{\tau}_A^{US}=1.462$ and $f(\tilde{\tau}_A^{US})=0.742$, and as we have seen already, Eq. (28) is not satisfied. The expected equilibrium transfer function is $f = 260.8/391.1 = 0.6668$, which corresponds to a global average water vapor column amount of 2.5 prcm. This value is about double of the actual amount.

Due to the low water vapor column amount in the USST-76 atmosphere the clear-sky estimates of the global average S_T , E_D , and E_U are unrealistic. The flux transmittance is over estimated by 33% and for example E_D is under estimated by about 31 W m^{-2} . The ERBE clear-sky OLR may also have a 6.5% positive bias. Although Eqs. (4) and (8) are satisfied, this discrepancy indicates that the USST-76 atmosphere does not represent a real radiative equilibrium temperature profile and should not be used as a single-column model for global energy budget studies.

It follows from Eq. (28) that $\pi B_0 = OLR(1-T_A)/2 = OLR(1+\hat{\tau}_C/2)$ and the characteristic optical depth will be equal to the total flux absorptance A . Those optical depths where the source function is equal to E_U or E_D can also be easily

derived: $\hat{\tau}_{E_U} = A - 2T_A/f$ and $\hat{\tau}_{E_D} = (2A/f) - T_A - 1$. Using large number of radiosonde observations, the global averages of πB_0 , E_U , OLR , E_D , S_U , and their respective optical depths can be computed, and one can establish the dependence of optical depth on the z geometric altitude. In *Fig. 5*, on the right vertical axis, the 0, $\hat{\tau}_{E_U}$, $\hat{\tau}_C$, $\tilde{\tau}_A^C$, $\hat{\tau}_{E_D}$, and $\tilde{\tau}_A^E$ optical depths are also indicated. Note the close to linear relationship between the altitude and the optical depth. This relationship may be represented pretty well by the $\hat{\tau}(z) = \tilde{\tau}_A(1 - z/10)$ equation, where z is given in km. This linear function directly contradicts to the usual assumption of exponential decrease of $\tilde{\tau}(z)$ function, indicating the different nature of $\hat{\tau}(z)$. The optical depth computed from Eq. (21) is essentially the measure of the transfer of heat energy by non radiative processes and can be regarded as a kind of dynamical flux optical depth. Although $\hat{\tau}(0) = \tilde{\tau}_A$, the $\tilde{\tau}(z) = -\ln(T_A(z))$ is an exponential function and the $T_A(z)$ is a linear function. Let us mention that a linear $\hat{\tau}(z)$ function is consistent with the hydrostatic equation: $dp/d\hat{\tau} = g_a/\hat{k}$, where p is the atmospheric pressure, g_a is the gravity acceleration, and \hat{k} is an effective absorption coefficient associated with $\hat{\tau}(z)$.

6. Error estimates

Eq. (28) was extensively validated against the results of large scale LBL simulations of the planetary flux optical depth and greenhouse effect, and selected satellite observations in *Miskolczi and Mlynczak (2004)*. In *Fig. 7* we summarize the errors of the semi-infinite approximation using Eqs. (16), (17), and (28). The comparison with Eq. (24) would be more complex, it involves real (or imposed) surface temperature discontinuity (through the term of S_G) and will be discussed elsewhere.

In the realistic range of the clear-sky $\tilde{\tau}_A$, Eq. (28) predicts 2–15% underestimates in the source function at the surface in Eq. (16), and about 25% overestimates in the surface upward radiation in Eq. (17). According to Eqs. (14) and (15), the response of the surface upward flux to a small optical depth perturbation, (CO_2 doubling, for example), is proportional to $\Delta\tilde{\tau}_A$. In the semi-transparent approximation $\Delta S_U(\tilde{\tau}_A) \approx \Delta\tilde{\tau}_A(1 - \exp(-\tilde{\tau}_A))$, which means that the semi-infinite approximation will seriously overestimate ΔS_U .

At a global average clear-sky optical depth the relative error is around 20%, but for smaller optical depth (polar areas) the error could well exceed 60%. Differences of such magnitude may warrant the re-evaluation of earlier greenhouse effect estimates. For the estimation of the greenhouse effect at some point all atmospheric radiative transfer model has to relate the flux optical depth (or absorber amount) to the source function, therefore one should be aware of the errors they might introduce to their results when applying the semi-infinite

approximation. The above sensitivity estimates assume a constant OLR , therefore, they should be regarded as initial responses for small optical depth perturbations. Considering the changes in the OLR as well, the correct theoretical prediction is $\Delta S_U / \Delta \tilde{\tau}_A = (A/4)OLR$.

For example, a hypothetical CO_2 doubling will increase the optical depth (of the global average profile) by 0.0241, and the related increase in the surface temperature will be 0.24 K. The related change in the OLR corresponds to -0.3 K cooling. This may be compared to the 0.3 K and -1.2 K observed temperature changes of the surface and lower stratosphere between 1979 and 2004 in *Karl et al.*, (2006).

From the extrapolation of the ‘Keeling Curve’ the estimated increase in the average CO_2 concentration during this time period is about 22% (*National Research Council of the National Academies*, 2004). Comparing the magnitude of the expected change in the surface temperature we conclude, that the observed increase in the CO_2 concentration must not be the primary reason of the global warming.

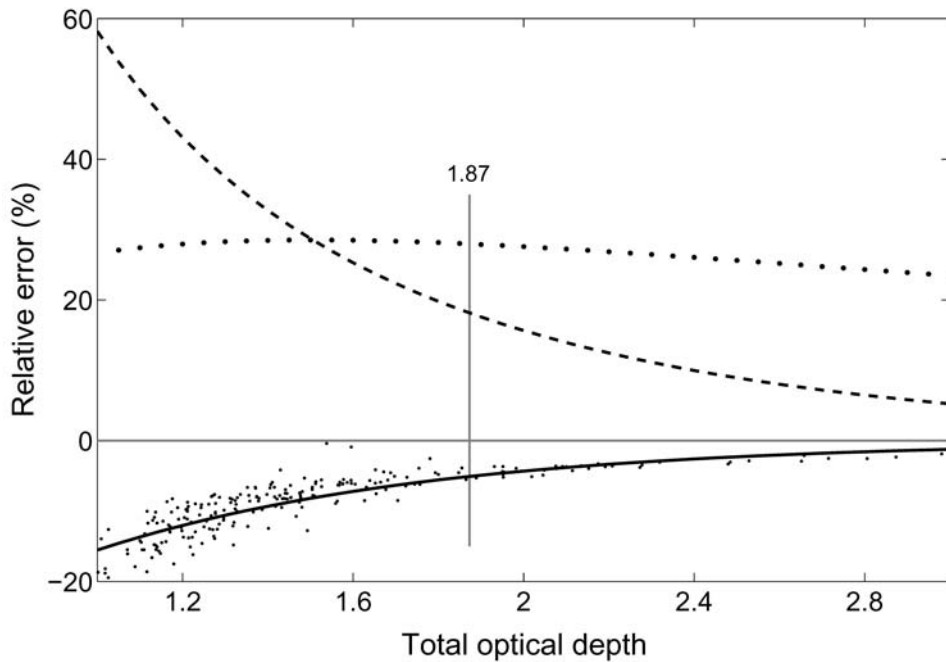


Fig. 7. The three relative error curves are: $f(\tilde{\tau}_A)[(1 + \tilde{\tau}_A)/2 - 1/f(\tilde{\tau}_A)]$ (solid line), $f(\tilde{\tau}_A)[1 + \tilde{\tau}_A/2 - 1/f(\tilde{\tau}_A)]$ (dotted line), and $1/(\exp(\tilde{\tau}_A) - 1)$ (dashed line). These functions represent the relative differences using Eqs. (16) and (17) or Eq. (28) for the computation of $S_U(\tilde{\tau}_A)$ and $\Delta S_U(\tilde{\tau}_A)$, respectively. The vertical line is an estimate of the clear-sky global average $\tilde{\tau}_A$. The dots represent 228 LBL simulation results. The scatter of the dots is due to the fact that the temperature profiles were not in perfect radiative equilibrium.

The f and g functions may be used for the theoretical interpretation of some empirical greenhouse parameters: $G_1 = G_N = g$, and $G_2 = S_U / OLR = 1/f$. Here G_1 is Raval and Ramanathan's normalized greenhouse parameter, and G_2 is Stephens and Greenwald's greenhouse parameter (Raval and Ramanathan, 1989; Stephens and Greenwald, 1991). The sensitivity of the greenhouse function to optical depth perturbations is expressed by the derivative of g :

$$g_S = dg / d\tilde{\tau}_A = f^2 A / 2. \quad (29)$$

The g_S function has a maximum at $\tilde{\tau}_A^S = 1.0465$, therefore, positive optical depth perturbations in the real atmosphere are coupled with reduced greenhouse effect sensitivity. Here we note, that the $g_S^\circ = 2T_A/5$ and $g_S^* = T_A/3$ sensitivities are decreasing monotonously with increasing $\tilde{\tau}_A$. It is also important that, due to the compensation effect of the combined linear and exponential optical depth terms, the f and g functions have negligible temperature dependence. There is, however, a slight non-linear dependence on the surface temperature introduced by the weighting of the monochromatic flux transmittances with the spectral S_U . Note, that the f and g functions can not be related easily to the absorber amounts, and, for example, a simple linear parameterization of them with the water vapor column amount could be difficult and inaccurate (Stephens and Greenwald, 1991; Miskolczi and Mlynczak, 2004).

The greenhouse parameters are dependent only on the flux optical depth, therefore it is difficult to imagine any water vapor feedback mechanism to operate on global scale. The global average $\tilde{\tau}_A^E$ is set by the global energy balance requirement of Eqs. (8) and (9).

It follows from Eqs. (8) and (28) that $3OLR/2 = OLR/f$ and $f = 2/3 = f^+$, giving an equilibrium optical depth of $\tilde{\tau}_A^+ = 1.841$. Using Eq. (9) and (28) the equilibrium optical depth becomes $\tilde{\tau}_A^\circ = 1.867$. The $\tilde{\tau}_A^E = 1.87$ is consistent with these theoretical expectations and the estimate of 1.79 in Section 3. The excess optical depth $\tilde{\tau}_A^E - \tilde{\tau}_A^+ = 0.029$ corresponds to about 1.5 W m^{-2} imbalance in S_U , which may temporarily be compensated for example by 1.0 W m^{-2} net heat flow from the planetary interior or by small decrease in the SW system albedo. In case of Eq. (9) the optical depth difference is even smaller, $\tilde{\tau}_A^E - \tilde{\tau}_A^\circ = 0.003$.

Since the world oceans are virtually unlimited sources and sinks of the atmospheric water vapor (optical depth), the system – depending on the time constant of the different energy reservoirs – has many ways to restore the equilibrium situation and maintain the steady state global climate. For example, in case the increased CO_2 is compensated by reduced H_2O , then the general circulation has to re-adjust itself to maintain the meridional energy flow with less water vapor available. This could increase the global average rain rate and speed up the global water cycle resulting in a more dynamical climate, but still

the energy balance equations do not allow the average surface temperature to rise. The general circulation can not change the global radiative balance although, changes in the meridional heat transfer may result in local or zonal warming or cooling which again leads to a more dynamical climate. Note that there are accumulating evidence of long term negative surface pressure trends all over the Southern Hemisphere (*Hines et al.*, 2000), which may be an indication of decreasing water vapor amount in the atmosphere.

The estimation of the absolute accuracy of the simulated global average $\tilde{\tau}_A^E$ is difficult. The numerical errors in the computations are negligible, and probably the largest single source of the error is related to the selection of the representative atmospheric profile set. To decide whether the indicated small optical depth differences are real, further global scale simulations are required.

In the view of the existence of the $\tilde{\tau}_A^+$ and $\tilde{\tau}_A^\circ$ critical optical depth, the runaway greenhouse theories have very little physical foundations. Greenhouse gases in any planetary atmosphere can only absorb the thermalized available SW radiation and the planetary heat flux. Keeping these flux terms constant, deviations from $\tilde{\tau}_A^+$ or $\tilde{\tau}_A^\circ$ will introduce imbalance in Eqs. (8) and (9), and sooner or later – due to the energy conservation principle – the global energy balance must be restored. On the long run the general energy balance requirement of Eq. (9) obviously overrules the IR radiative balance requirement of Eq. (28).

Based on Eq. (28) we may also give a simple interpretation of E_U : $E_U = S_U f - S_U T_A$. Since the total converted $F^0 + P^0$ to OLR is $S_U f$, and $S_U T_A$ is the transmitted part of the surface radiation, the $S_U f - S_U T_A$ difference is the contribution to the OLR from all other energy transfer processes which are not related to LW absorption: $E_U = F + K + P$. Substituting this last equation into the energy balance equation at the lower boundary, and using Eq. (3) we get: $E_D - A_A = 0$. This is the proof of the Kirchhoff law for the surface-atmosphere system. The validity of the Kirchhoff law requires the thermal equilibrium at the surface. Note, that in obtaining Eq. (28) the Kirchhoff law was not used (see Appendix B).

8. Zonal distributions

To explore the imbalance caused by optical depth perturbations, one has to use the differential form of Eq. (28):

$$\Delta f / f = \Delta OLR / OLR - \Delta S_U / S_U. \quad (30)$$

According to Eq. (30) the relative deviations from the equilibrium f , OLR , and S_U must be balanced. The validity of Eq. (30) is nicely demonstrated in *Fig. 8*.

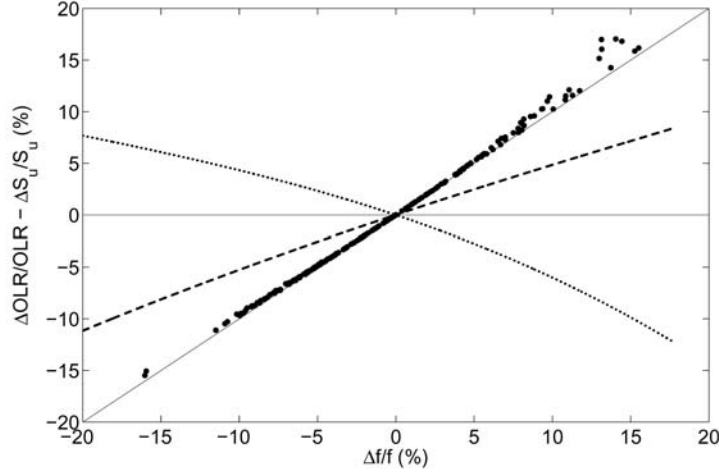


Fig. 8. Validation of the $\Delta f/f = \Delta OLR/OLR - \Delta S_U/S_U$ equation. Dots were computed from radiosonde observations and they represent the relative differences from the equilibrium f . The dashed and dotted lines are fitted to the $\Delta OLR/OLR$ and $\Delta S_U/S_U$ points, respectively.

The Δf can be related to the $\Delta \tilde{\tau}_A$ quantity through the $\Delta f = -\Delta \tilde{\tau}_A f^2 A/2$ equation. The ΔOLR and ΔS_U quantities are defined by the next two equations: $\Delta OLR = -S_U \Delta \tilde{\tau}_A f^2 A/4$ and $\Delta S_U = OLR \Delta \tilde{\tau}_A A/4$. It can be shown that the $\Delta OLR/OLR + \Delta S_U/S_U = 0$, and $\Delta OLR = -f \Delta S_U$ equations also hold. In Fig. 9 the dependence of ΔS_U on ΔOLR is presented. The open circles in this figure indicate small deviations from Eq. (30). At larger $|\Delta S_U|$ the true ΔOLR is slightly overestimated. Figs. 8 and 9 show that the surface warming is coupled with reduced OLR , which is consistent with the concept of the stratospheric compensation.

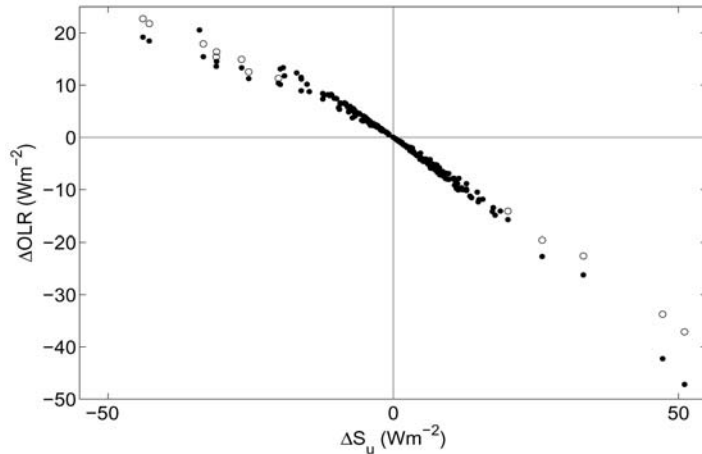


Fig. 9. The imbalance in S_U and OLR are marked with black dots. For the $|\Delta S_U| > 20 \text{ W m}^{-2}$ the open circles were computed from the $\Delta OLR = -f \Delta S_U$ equation.

Unfortunately, our static model can not deal with the dynamical factors represented by the variables K and F . The decomposition of E_U into its several components is beyond the scope of this study. Based on our large scale clear-sky

simulations, in *Figs. 10, 11, and 12* we present the meridional distributions of the zonal mean $\tilde{\tau}_A$, OLR , and S_U , and their deviations from Eqs. (8) and (28).

In *Fig. 10* the zonal average $\tilde{\tau}_A$ distributions are presented. At the equatorial regions up to about ± 35 degree latitudes, the atmosphere contains more water vapor than the planetary balance requirement of $\tilde{\tau}_A^+$. This feature is the result of the combined effects of evaporation/precipitation processes and the transport of the latent and sensible heat by the general circulation. The reason of the differences between the actual and equilibrium zonal distributions is the clear-sky assumption. The global averages for both distributions are 1.87 representing about 2.61 prcm global average water vapor column amount.

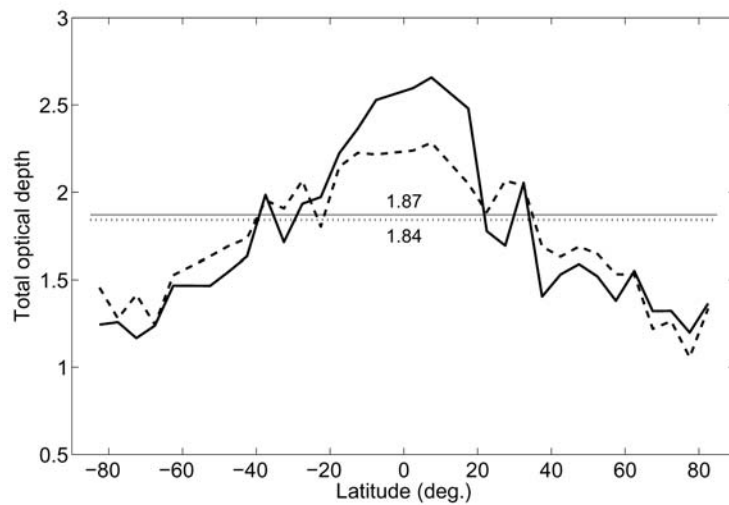


Fig. 10. Meridional distributions of the zonal mean clear sky $\tilde{\tau}_A$. Solid line is the actual $\tilde{\tau}_A$ computed from simulated flux transmittance. Dashed line is the required $\tilde{\tau}_A$ to satisfy the $2S_U/OLR - 1 = \tilde{\tau}_A + \exp(-\tilde{\tau}_A)$ equation. Thin solid horizontal line is the global average for both curves. Dotted line is the planetary equilibrium optical depth, $\tilde{\tau}_A^+$, obtained from Eqs. (6) and (26).

In *Fig. 11* the simulated OLR and the fS_U theoretical curve show good agreement at higher latitudes, indicating that for zonal means the IR radiative balance holds. At the equatorial regions the simulations significantly overestimate fS_U . The reason is the un-accounted cloud cover at low latitudes. The dotted line is the required OLR to completely balance the zonal mean S_U and can be regarded as the zonal mean clear-sky F^0 .

In *Fig. 12* again, the effect of the cloud cover at low latitudes is the reason of the theoretical overestimation of S_U . At high latitudes Eq. (28) approximately holds. The dots were computed using the semi-infinite model, and they show significant underestimation in the observed zonal mean S_U . According to *Figs. 11 and 12*, at higher latitudes the flux densities are almost balanced.

The quantitative analysis and the explanation of the imbalance at the equatorial regions requires further investigation involving large-scale

simulations of cloudy atmospheres. It is also necessary to build a suitable theoretical broad band radiative transfer model for studying the different aspects of a complex multi-layer cloud cover. Using the new equations there is a hope that simple bulk formulation may be developed to deal with the planetary scale energetics of the cloud cover.

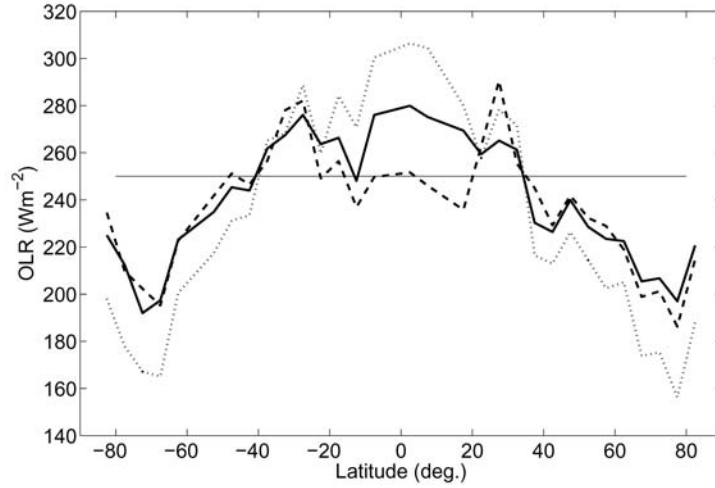


Fig. 11. Meridional distributions of the zonal mean OLR . Solid line is the actual clear-sky OLR computed from all sky radiosonde observations. Dashed line is the required $OLR = f S_U$ equation. The horizontal line is the global average. Dotted line is the zonal mean equilibrium OLR computed as $2S_{Tl}/3$.

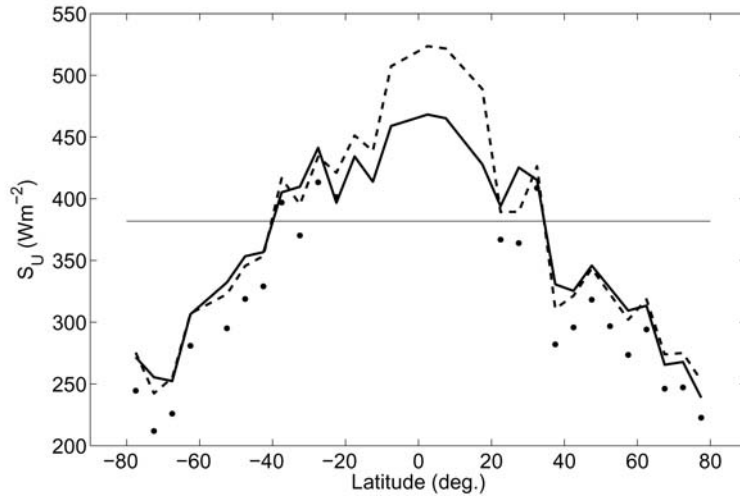


Fig. 12. Meridional distributions of the zonal mean surface upward flux densities. Thick solid line is the observed all sky S_U . Dashed line is the required S_U to satisfy the $S_U = OLR/f$ equation. Thin solid horizontal line is the global average. Dots represent the semi-infinite approximation of $S_U = OLR(1 + \bar{\tau}_A)/2$ for higher latitudes.

The f , $f - T_A$, and g functions can be regarded as theoretical normalized radiative flux components representing OLR/S_U , E_U/S_U , and $(S_U - OLR)/S_U$ ratios, respectively. The f° , $f^\circ - T_A$, g° , and f^* , $f^* - T_A$, and g^* are similar functions representing Eqs. (9) and (10), respectively. The dependences of these

functions and the g_S function on the optical depth are presented in *Fig. 13*. For reference, in this figure we also plotted the individual simulation results of E_U/S_U for the Earth and Mars, and the OLR/S_U only for the Mars. In the next sections we discuss some further characteristics of the broadband IR atmospheric radiative transfer of Earth and Mars.

At this time the Venusian atmosphere is not included in our study. The major problem with the Venusian atmosphere is the complete cloud cover and the lack of knowledge of the accurate surface SW and LW fluxes. The development of a comprehensive all-sky broadband radiative transfer model is in progress.

9.1 Earth

In *Fig. 13* the simulated global average normalized flux densities are very close to the theoretical curves, proving that the new equations reproduce the real atmospheric situations reasonably well. The horizontal scatter of the gray dots indicate the range of the optical depth that characteristic for the Earth's climate. Theoretically, the lower limit is set by the minimum water vapor amount and the CO₂ absorption. The upper limit is set by a theoretical limiting optical depth of $\tilde{\tau}_A^L = 2.97$, where the transfer and greenhouse functions becoming equal. This optical depth corresponds to about 6 prcm water vapor column amount, which is consistent with the observed maximum water vapor content of a warm and humid atmosphere.

The vertical scatter of the gray dots around the $f - T_A$ curve is the clear indication that locally the atmosphere is not in perfect radiative equilibrium and Eq. (28) is not perfectly satisfied. The obvious reason is the SW effect of the cloud cover and the more or less chaotic motion of the atmosphere. For the global averages Eqs. (8) and (28) represent strict radiative balance requirements. On regional or local scale this equation is not enforced by any physical law and we observe a kind of stochastic radiative equilibrium which is controlled by the local climate.

Over a wide range of optical depth around $\tilde{\tau}_A^U$, the $f - T_A$ curve is close to 0.5, which assures that E_U is approximately equal to $S_U/2$ independently of the gravitational constraint (virial theorem). This explains why Eqs. (9) and (25) can co-exist at the same $\tilde{\tau}_A^E$. The USST-76 atmosphere seems to follow the radiation scheme of Eqs. (8), $OLR/S_U \approx 2/3$. At the $\tilde{\tau}_A^{US}$ the global radiative balance of the atmosphere is violated and the atmosphere can not be in radiative equilibrium either. The radiative balance and the radiative equilibrium can not co-exist at $\tilde{\tau}_A^{US}$. The radiative imbalance may be estimated from Eqs. (8) and (9) as $S_U(2/3 - (1 - 2A/5)) \approx -10 \text{ W m}^{-2}$. To retain the energy balance, the USST-76 atmosphere should lose about 10 W m^{-2} more IR radiation to space. The use of such atmospheres for global energy budget studies has very little merit.

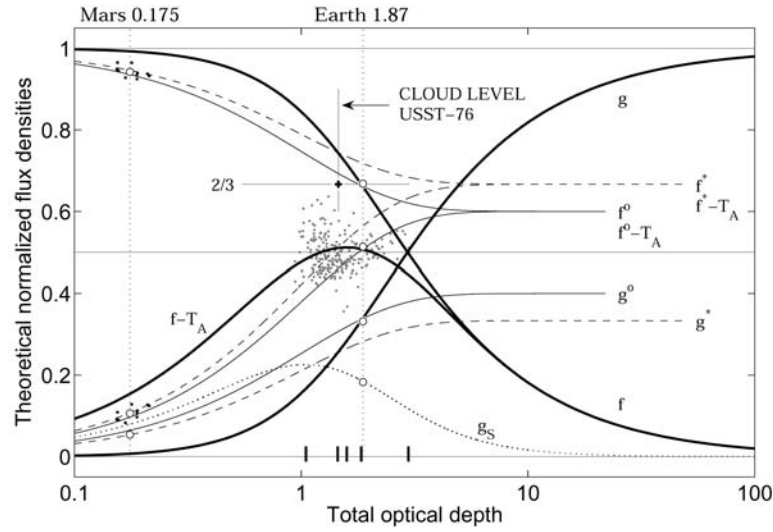


Fig. 13. Theoretical relative radiative flux ratio curves. Open circles are computed planetary averages from simulations. The individual simulation results of E_U/S_U are shown as gray dots for the Earth and black dots in the lower left corner for the Mars. The black dots in the upper left corner are the simulated OLR/S_U for Mars. The g_S curve is the theoretical greenhouse sensitivity function for the Earth. The five short vertical markers on the zero line at the positions of 1.05, 1.42, 1.59, 1.84, and 2.97 are (from left to right) the locations of $\tilde{\tau}_A^S$, $\tilde{\tau}_A^C \approx \tilde{\tau}_A^{US}$, $\tilde{\tau}_A^U$, $\tilde{\tau}_A^+ \approx \tilde{\tau}_A^\circ$, and $\tilde{\tau}_A^L$ optical depths, respectively.

This figure shows that the Earth has a controlled greenhouse effect with a stable global average $\tilde{\tau}_A^E = 1.87 \approx \tilde{\tau}^+ \approx \tilde{\tau}^\circ$, $g(\tilde{\tau}_A^E) = 0.33 \approx g^+ \approx g^\circ(\tilde{\tau}_A^E)$, and $g_S(\tilde{\tau}_A^E) \approx 0.185$. As long as the $F^0 + P^0$ flux term is constant and the system is in radiative balance with a global average radiative equilibrium source function profile, global warming looks impossible. Long term changes in the planetary radiative balance is governed by the $F^0 + P^0 = S_U(3/5 + 2T_A/5)$, $OLR = S_U f$ and $F^0 + P^0 = OLR$ equations. The system is locked to the $\tilde{\tau}_A^\circ$ optical depth because of the energy minimum principle prefers the radiative equilibrium configuration ($\tilde{\tau}_A < \tilde{\tau}_A^\circ$) but the energy conservation principle constrains the available thermal energy ($\tilde{\tau}_A > \tilde{\tau}_A^\circ$). The problem for example with the highly publicized simple ‘bucket analogy’ of greenhouse effect is the ignorance of the energy minimum principle (*Committee on Radiative Forcing Effects on Climate Change et al.*, 2005).

According to Eq. (9), a completely opaque cloudless atmosphere ($T_A \approx 0$) would accommodate a surface temperature of $\bar{t}_S = 288.3$ K, which is pretty close to the observed global average surface temperature. In this extent the LW effect of the cloud cover is equal to closing the IR atmospheric window and increasing the global average greenhouse effect by about 1.8 K, without changing the $\tilde{\tau}_A^E \approx \tilde{\tau}_A^\circ$ relation. The $\beta \approx 0.6$ cloud cover simultaneously assures the validity of the $OLR^A = \bar{S}_U(1 - 2\bar{A}/5) \approx 3\bar{S}_U/5$ radiation balance equation with $\bar{A} \approx 1$ and a global average $\bar{S}_U = 392$ W m⁻², and the radiative equilibrium

clear-sky source function profile with $\tilde{\tau}_A^E = 1.87$. This could be the configuration, which maintains the most efficient cooling of the surface-atmosphere system.

9.2 Mars

We performed LBL simulations of the broadband radiative fluxes for eight Martian standard atmospheres. In *Fig. 14* the temperature and volume mixing ratio profiles are shown in the 0–60 km altitude range.

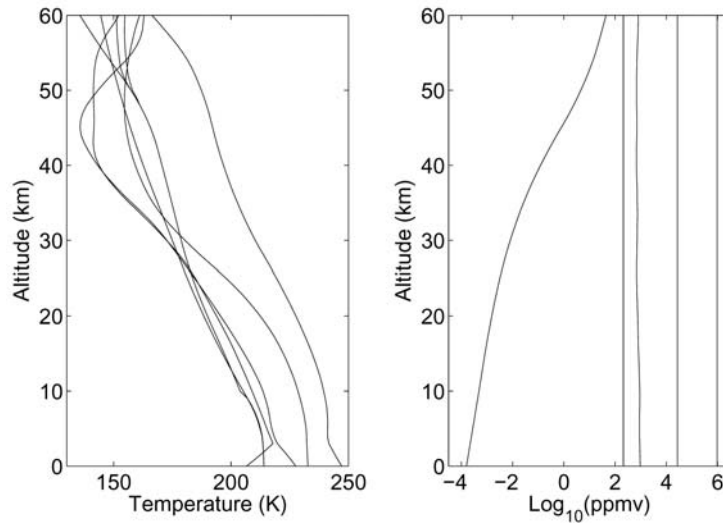


Fig. 14. Martian standard temperature and volume mixing ratio profiles. In the right plot the absorbers are (from left to right): O₃, H₂O, CO, N₂, and CO₂.

In *Fig. 15* dust-free clear-sky computed spectral OLR and S_U are presented for the coldest and warmest temperature profiles. The computations were performed in the 1–3490 cm^{-1} wavenumber range with 1 cm^{-1} spectral resolution. The single major absorption feature in these spectra is the 15 μ CO₂ band. The signatures of the 1042 cm^{-1} ozone band and several H₂O bands are present only in the upper (warmer) spectrum. Despite the almost pure CO₂ atmosphere, the clear Martian atmosphere is remarkably transparent. The average flux transmittance is $T_A = 0.839$ (just about equal to the flux absorptance on the Earth), and the OLR is largely made up from S_T .

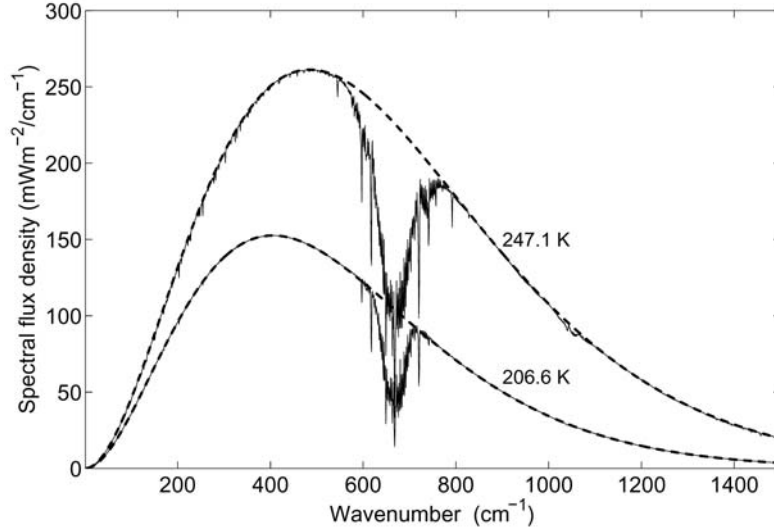


Fig. 15. LBL simulations of the spectral flux densities for a warm and a cold standard Martian atmospheric profile. The thin solid line is the spectral OLR and the thick dashed line is the blackbody function at the indicated surface temperatures.

In *Fig. 16* the relationships between S_U and S_T are shown for the Mars and Earth. In case of the Earth, S_T is almost independent of S_U , while in the Martian atmosphere the transmitted radiation depends linearly on the surface upward radiative flux. This fact is an indication that the broadband radiative transfer is fundamentally different on the two planets.

On Mars the optical depth has a strong direct dependence on the total mass of the atmosphere and consequently on surface pressure. The average flux optical depth is small, $\tilde{\tau}_A = 0.175 \ll \tilde{\tau}_A^+$. In *Fig. 13* the simulated OLR/S_U and E_U/S_U ratios systematically underestimate the theoretical f and $f - T_A$ functions. With the $P^0 \approx 0$ assumption, Mars does not satisfy the IR radiative equilibrium and the overall energy balance criteria at the surface.

For five model profiles the deviations from Eqs. (8) and (28) are presented in *Fig. 17*. The primary reason of the deviations related to the mechanism of the atmospheric heating by non IR radiative processes. On the Earth $K + F$ is large and sufficient to maintain the internal kinetic energy required by the surface pressure and the hydrostatic equilibrium ($E_U/S_U \approx 1/2$). The Martian atmosphere can not gain much energy through the K and F terms. The sublimation and condensation of CO_2 are mainly surface processes, no extended CO_2 cloud cover is observed. The visible and near IR absorption is also small, most of the SW flux is absorbed at the surface, consequently F is also small.

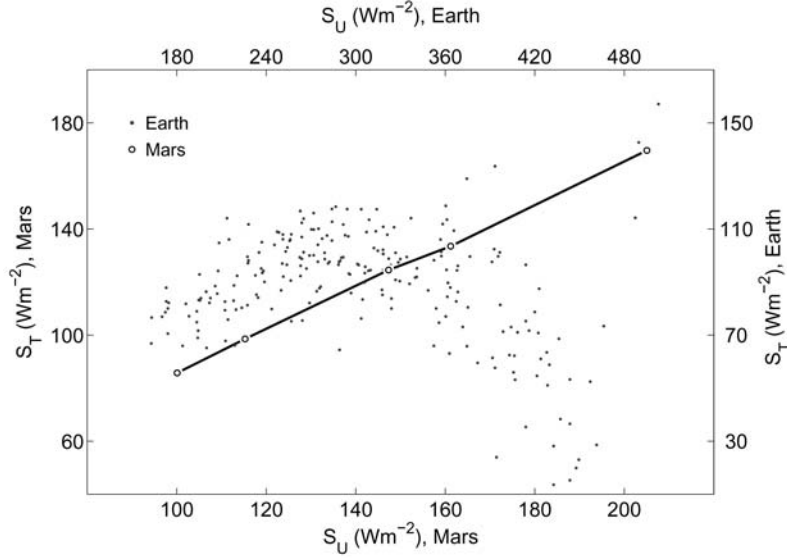


Fig. 16. Relationships between S_U and S_T . Data were obtained by LBL simulations using a set of Martian standard profiles and selected radiosonde observations from the TIGR radiosonde archive. In case of the Earth no significant linear correlation exists between S_U and S_T .

Simulation results show that the average E_U and S_U are 14.2 W m^{-2} and 134 W m^{-2} , respectively. The resulting $E_U/S_U \approx 0.1$ ratio is far too small to assure the hydrostatic equilibrium. In transparent atmospheres the $E_D/10$ term is usually small and may be ignored in Eq. (9). In case of Mars $E_D/10$ is about 1.5% of S_U , and apparently, the Martian atmosphere accommodates the radiative transfer scheme of Eq. (10).

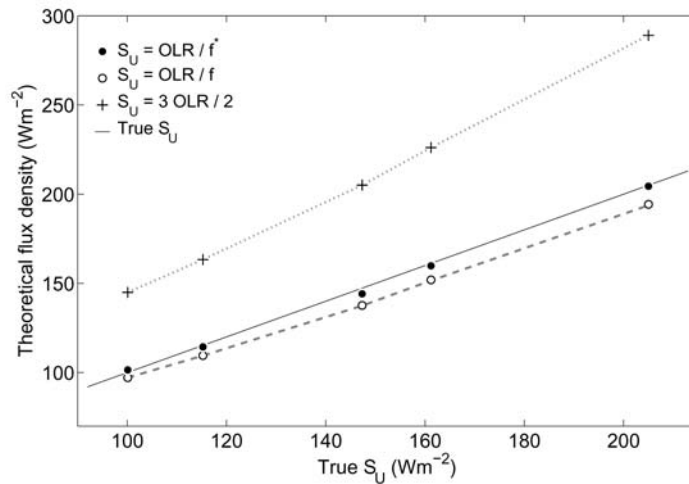


Fig. 17. Validation of the $f^* = 1 - A/3$ transfer function. The solid dots are the S_U fluxes computed with the new f^* transfer function. The 'true' S_U (solid line) were computed from the temperatures of the lowest levels of the standard Martian profiles via the Stefan-Boltzmann law. The 'o' and '+' symbols are the predictions of S_U using the f and the $S_U = 3OLR/2$ equations, respectively.

Using an average available absorbed SW radiation of 127 W m^{-2} Eq. (8) would require -56 W m^{-2} thermal energy to maintain the planetary energy balance. Simulation results show that S_T is 112.3 W m^{-2} and half of it could really restore the energy balance. Since the average E_U is small the $S_T/2$ flux term is the major contribution to the internal kinetic energy of the atmosphere. The wind blown atmospheric dust particles could have an important role in transferring this amount of thermal energy from the surface to the atmosphere. The f^* transfer function predicts both the true S_U in *Fig. 17* (solid dots) and the average relative OLR and E_U in *Fig. 13* (open circles) pretty well.

The linear dependence of $S_U f^*$ on $S_U T_A$ in *Fig. 16* explains why the band averaged spectral OLR/S_U ratio resolves the surface topography in the IR images in Chamberlain et al. (2006). The $f^* - T_A$ and g^* functions are also plotted in *Fig. 13*. The intersection of the f^* and f curves points to an optical depth of $\tilde{\tau}_A^* = 1.451$ where the atmosphere would be in radiative equilibrium with a linear average source function profile. At this $\tilde{\tau}_A^*$ the $E_D/10$ term in Eq. (9) becoming large, the approximation of Eq. (10) will not hold, and consequently the radiative balance can not exist. The error of Eq. (10) increases with increasing optical depth.

Regarding the range of the variability of the optical depth (or surface pressure) this situation can not occur in the clear Martian atmosphere. In the radiation scheme of Eq. (10) the runaway greenhouse effect is impossible, S_U will tend to $3OLR/2$ with increasing optical depth.

A further interesting consequence of Eq. (10) is the $2E_D - 3E_U = 0$ relationship. For the deeper understanding of these types of balance equations, in *Figs. 18* and *19* the spectral flux density differences are plotted around the central region of the $15 \mu\text{m}$ CO_2 absorption band.

In *Fig. 18* the band averaged differences of both the thick and thin solid curves are represented with a single dotted line at the zero position. We see that the spectral deviations of both the $S_U - OLR/f^*$ and $3OLR/2 - (S_U + S_T/2)$ spectral differences are almost perfectly compensated, assuring the validity of the respective balance equations. In *Fig. 19* similar explanation holds for the validity of the $2E_D - 3E_U = 0$ relationship. In this case the integral of the spectral $2E_D - 3E_U$ over the $1-3490 \text{ cm}^{-1}$ range is 0.04 W m^{-2} only.

The average normalized greenhouse factor G_N is 0.0522 , which is consistent with the $A/3 = 0.0536$ theoretical value. The $G = 7.1 \text{ W m}^{-2}$ greenhouse factor gives 3 K greenhouse enhancement to the planetary average surface temperature. The greenhouse sensitivity is $df^*/d\tilde{\tau}_A = T_A/3 = 0.23$ per unit optical depth and always decreasing with increasing $\tilde{\tau}_A$.

We may conclude, that Eq. (10) adequately describes the broadband radiative fluxes in the Martian atmosphere, but for planets with significantly larger optical depths Eq. (9) must be used.

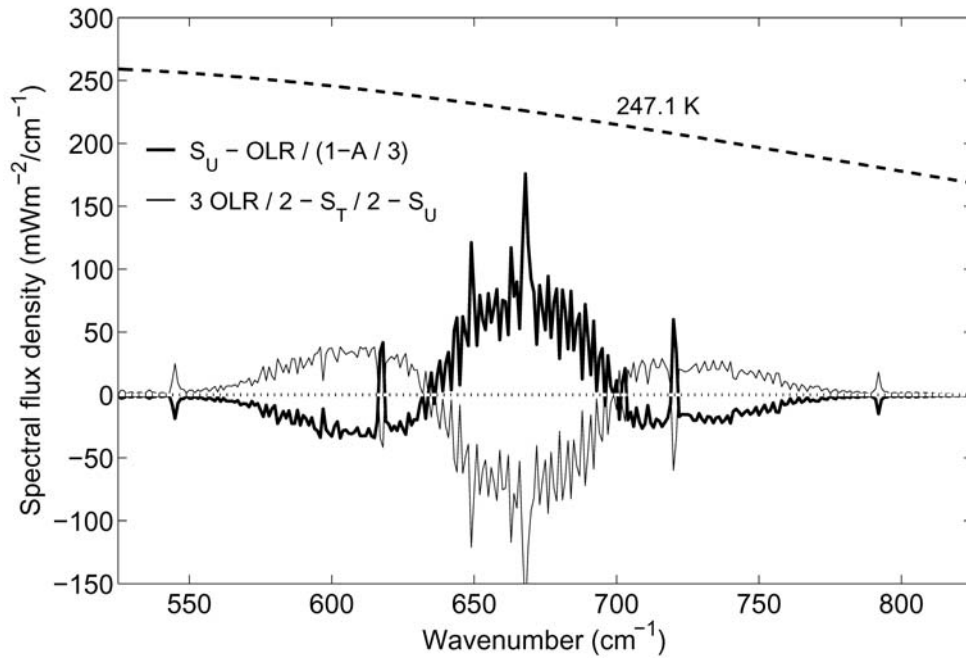


Fig. 18. Spectral flux differences in the $15 \mu\text{m}$ CO_2 band. The dotted line represents the averaged differences over the $1\text{--}3490 \text{ cm}^{-1}$ spectral range for both curves. The dashed line is the spectral blackbody radiation at the indicated surface temperature. The spectral differences are compensated over a relatively narrow wavenumber interval around the band center.

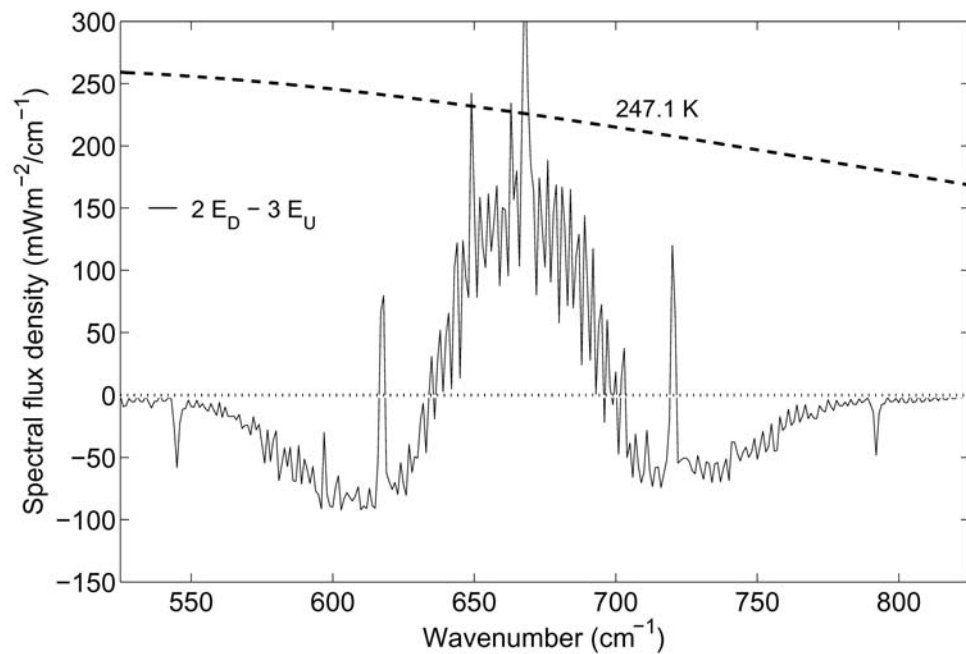


Fig. 19. Spectral differences in the $2E_D$ and $3E_U$ flux densities. The dotted line represents the averaged differences over the $1\text{--}3490 \text{ cm}^{-1}$ spectral range. The dashed line is the spectral blackbody function at the indicated surface temperature. The spectral differences are largely compensated over the extent of the $15 \mu\text{m}$ CO_2 band.

10. Conclusions

The purpose of this study was to develop relevant theoretical equations for greenhouse studies in bounded semi-transparent planetary atmospheres in radiative equilibrium. In our terms the local radiative equilibrium is a unique instantaneous state of the atmosphere where the upward atmospheric radiation is balanced by the short wave atmospheric absorption and the net exchange of thermal fluxes of non-radiative origin at the boundary. In general, the thermal structure of the atmosphere assures that the absorbed surface upward radiation is equal to the downward atmospheric radiation. It seems that the Earth's atmosphere maintains the balance between the absorbed short wave and emitted long wave radiation by keeping the total flux optical depth close to the theoretical equilibrium values.

On local scale the regulatory role of the water vapor is apparent. On global scale, however, there can not be any direct water vapor feedback mechanism, working against the total energy balance requirement of the system. Runaway greenhouse theories contradict to the energy balance equations and therefore, can not work. We pointed to the importance of a characteristic altitude of about 2 km, where the cloud cover may control the SW input of the system without changing the global average OLR . To explain the observed increase in the global average surface temperature probably more attention should be paid to the changes in the net contribution from the F^0 and P^0 flux terms and changes in the global average water vapor content and cloud cover. Instead of the USST-76 atmosphere, further global energy budget studies should use appropriate zonal and global average atmospheres which satisfy the global radiative balance requirement and comply with the physics of the global greenhouse effect.

Eqs. (21) and its derivatives are theoretically sound and mathematically correct relationships between the fluxes, greenhouse parameters, and the flux optical depths, and they are good enough to give quantitative estimates with reasonable accuracy. One of the most important results is the derived $S_U = OLR/f$ functional relationship which replaces the mathematically incorrect $S_A = OLR(1 + \tilde{\tau}_A)/2$ and $S_G = OLR(2 + \tilde{\tau}_A)/2$ equations (classic Eddington solutions), and also resolves the surface temperature discontinuity problem. In radiative equilibrium the thermal equilibrium at the surface is the consequence of the energy minimum principle and it is an explicit requirement of the new equations.

We showed that, by applying the semi-infinite atmospheric model for clear or optically thin atmospheres, large errors may be introduced into the equilibrium surface temperatures. An other important consequence of the new equations is the significantly reduced greenhouse effect sensitivity to optical

depth perturbations. Considering the magnitude of the observed global average surface temperature rise and the consequences of the new greenhouse equations, the increased atmospheric greenhouse gas concentrations must not be the reason of global warming. The greenhouse effect is tied to the energy conservation principle through the $S_U + S_T/2 - E_D/10 = 3(F^0 + P^0)/2 = 3S_U f/2$ equations and can not be changed without increasing the energy input to the system.

Applying the virial theorem new radiative balance equations were derived. We showed that the clear Martian model atmospheres are not in radiative equilibrium. The new transfer and greenhouse functions adequately describe the planetary greenhouse effect on the Mars and Earth. The formulation of the new theory for the completely cloudy Venusian atmosphere is in progress.

The basic limitations of our formulas are related to the Eddington, and LTE approximations, and – regarding the practical applications – the assumption of the radiative balance and radiative equilibrium. The simplicity and compactness of the formulas make the flux calculations easy and fast and make them good candidates for greenhouse effect parameterizations in sophisticated climate models. Reasonable global change assessment using GCMs is only possible by observing the basic physical principles governing the planetary greenhouse effect. Regarding the economical impact of the global warming the identification of the real causes of the warming should have the highest priority of the climate research. We believe that the fundamental physics of the greenhouse effect in semi-transparent planetary atmospheres is clearly reflected in the new equations and once the new greenhouse theory may even appear in textbooks on the atmospheric radiative transfer.

Acknowledgements—It is my privilege to publish this paper in the *Időjárás*. I wish to thank for the support and encouragement obtained from *G. Major, Sz. Barcza, Z. Tóth, M. Zágoni, L. Bozó, K. Sifrin, K. Rutledge, K. Vinnikov, and S. Gupta*. I am also very grateful to *M. Antal* for her help with the final editing of the manuscript.

Appendix A: Flux optical depth

The usual definition of the gray-body optical depth is the $d\bar{\tau} = \bar{k} du$ equation, where \bar{k} is a properly averaged absorption coefficient over the wavenumber domain, and u is the total amount of a particular absorber along the optical path. Regarding an S_0 LW radiative flux passing through a homogeneous absorbing layer, it is expected that the transmitted part of S_0 satisfies the next equations: $S(\bar{\tau}) = S_0 \exp(-\bar{\tau}) = S_0 \exp(-\bar{k}u)$ and $S(0) = S_0$. In general, for a mixture of different kind of absorbers having complex overlapping rotational-vibrational band structures no such weighted average absorption coefficient (and effective absorber amount) can be computed a-priori. However, for an inhomogeneous layered atmosphere the exact flux optical depth may be obtained by using the

LBL method. The first step is to compute the directional mean transmittances over a suitable short wavenumber interval:

$$\bar{T}_A(\Delta\nu, \mu) = \frac{1}{\Delta\nu} \int_{\Delta\nu} \exp\left[-\sum_{l=1}^L \sum_{i=1}^N \left[c^{i,l} + k_\nu^{i,l} \right] \frac{u^{i,l}}{\mu^l} \right] d\nu, \quad (\text{A1})$$

where $\mu^l = \cos(\theta^l)$ and θ^l is the local zenith angle, $c^{i,l}$ and $k_\nu^{i,l}$ are the contributions to the total monochromatic absorption coefficient from the continuum type absorptions and all absorption lines relevant to the i th absorber and l th layer, respectively. $N=11$ is the total number of major absorbing molecular species and $L=150$ is the total number of the homogeneous atmospheric layers. In HARTCODE the wavenumber integration is performed numerically by 5th order Gaussian quadrature over a wavenumber mesh structure of variable length. At least $\Delta\nu = 1 \text{ cm}^{-1}$ spectral resolution is required for the accurate Planck weighting. The hemispheric spectral flux transmittance is obtained by integrating Eq. (A1) with respect the solid angle:

$$\tilde{T}_A(\Delta\nu) = \int_{2\pi} \bar{T}_A(\Delta\nu, \mu) d\omega. \quad (\text{A2})$$

In the computation of the integral in Eq. (A2) nine streams (zenith angles) were used and the cylindrical symmetry of the radiation field was also assumed. The Planck-weighted hemispheric mean transmittances were computed from $\tilde{T}_A(\Delta\nu)$ by the following sum:

$$T_A = \frac{1}{\sigma t_A^4} \sum_{j=1}^M \pi B(\Delta\nu_j, t_A) \tilde{T}_A(\Delta\nu_j), \quad (\text{A3})$$

where $M=3490$ is the total number of spectral intervals, t_A is the surface temperature, and $B(\Delta\nu_j, t_A)$ is the averaged Planck function over $\Delta\nu_j$. Since the sum in Eq. (A3) is obviously the total transmitted radiative flux from the ground, the exact flux optical depth may be expressed as:

$$\tilde{\tau}_A = -\ln(T_A). \quad (\text{A4})$$

The dependence of $\tilde{\tau}_A$ on the individual total absorber amounts still can not be computed directly, but using a pre-computed database the construction of a $\tilde{\tau}_A(u^1, u^2, \dots, u^N)$ function is a matter of a multi-dimensional parameterization. Here u^1, \dots, u^N represent the column amounts of the different greenhouse gases. Such parameterization may also contain the effective temperature and pressure of the absorbers.

Appendix B: Source function profile in bounded atmosphere

We have seen that in a semi-transparent atmosphere the surface upward radiation is $B_G = \varepsilon_G \sigma t_G^4 / \pi$, and the upper boundary condition at the top of the atmosphere is the zero downward IR radiance. The upward and downward hemispheric mean radiance at the upper boundary using the general classic solution of the plane-parallel radiative transfer equation and the isotropy approximation are:

$$\bar{I}^+(0) = B_G e^{-\frac{3}{2}\bar{\tau}_A} + \frac{3}{2} \int_0^{\bar{\tau}_A} B(\bar{\tau}') e^{-\frac{3}{2}\bar{\tau}'} d\bar{\tau}', \quad (\text{B1})$$

and

$$\bar{I}^-(0) = 0. \quad (\text{B2})$$

Putting Eq. (B1) and Eq. (B2) into the $H(\bar{\tau}) = \pi(\bar{I}^+ - \bar{I}^-)$ equation, and substituting the source function with $B(\bar{\tau}) = 3H(\bar{\tau})/(4\pi) + B_0$ in the upward hemispheric mean radiance we get:

$$\frac{H}{\pi} = B_G e^{-\frac{3}{2}\bar{\tau}_A} + \frac{3}{2} \int_0^{\bar{\tau}_A} \frac{3H}{4\pi} \bar{\tau}' e^{-\frac{3}{2}\bar{\tau}'} d\bar{\tau}' + \frac{3}{2} \int_0^{\bar{\tau}_A} B_0 e^{-\frac{3}{2}\bar{\tau}'} d\bar{\tau}'. \quad (\text{B3})$$

The two definite integrals in the second and third terms of the right hand side of Eq. (B3) must be evaluated:

$$\frac{3}{2} \int_0^{\bar{\tau}_A} \frac{3H}{4\pi} \bar{\tau}' e^{-\frac{3}{2}\bar{\tau}'} d\bar{\tau}' = -\frac{H}{4\pi} (2e^{-\frac{3}{2}\bar{\tau}_A} - 2 + 3\bar{\tau}_A e^{-\frac{3}{2}\bar{\tau}_A}), \quad (\text{B4})$$

$$\frac{3}{2} \int_0^{\bar{\tau}_A} B_0 e^{-\frac{3}{2}\bar{\tau}'} d\bar{\tau}' = B_0 (1 - e^{-\frac{3}{2}\bar{\tau}_A}). \quad (\text{B5})$$

After putting back Eqs. (B4) and (B5) into Eq. (B3) we get:

$$\frac{H}{\pi} = B_G e^{-\frac{3}{2}\bar{\tau}_A} + \frac{H}{4\pi} (2e^{-\frac{3}{2}\bar{\tau}_A} - 2 + 3\bar{\tau}_A e^{-\frac{3}{2}\bar{\tau}_A}) + B_0 (1 - e^{-\frac{3}{2}\bar{\tau}_A}). \quad (\text{B6})$$

Rearranging Eq. (B6) and using the $\tilde{\tau}_A = (3/2)\bar{\tau}_A$ notation for the total flux optical depth, πB_0 can be expressed as:

$$\pi B_0 = \frac{\frac{H}{2} \left[1 + \tilde{\tau}_A e^{-\tilde{\tau}_A} + e^{-\tilde{\tau}_A} \right] - \pi B_G e^{-\tilde{\tau}_A}}{1 - e^{-\tilde{\tau}_A}}. \quad (\text{B7})$$

This B_0 in the $B(\bar{\tau}) = 3H(\bar{\tau})/(4\pi) + B_0$ equation will give the general form of the source function profile:

$$\pi B(\tilde{\tau}) = \frac{\frac{H}{2} \left[1 + \tilde{\tau} + (\tilde{\tau}_A - \tilde{\tau} + 1)e^{-\tilde{\tau}_A} \right] - \pi B_G e^{-\tilde{\tau}_A}}{1 - e^{-\tilde{\tau}_A}}. \quad (\text{B8})$$

Applying the $T_A = \exp(-\tilde{\tau}_A)$, $A = 1 - T_A$, and $f = 2/(1 + \tilde{\tau}_A + Tr_A)$ notations, Eq. (B8) will become identical with Eq. (21). The semi-infinite solution may be obtained exactly in the same way, but substituting $\tilde{\tau}_A$ with infinity in Eq. (B1), or simply by making these substitutions in Eq. (B8).

The most efficient cooling of the clear atmosphere requires a total optical depth that maximizes B_0 . The derivative of Eq. (B7) with respect $\tilde{\tau}_A$ may be expressed as:

$$\pi \frac{dB_0(\tilde{\tau}_A)}{d\tilde{\tau}_A} = \frac{d}{d\tilde{\tau}_A} \left[\frac{\frac{OLR}{2} \left[1 + \tilde{\tau}_A + e^{\tilde{\tau}_A} \right] - \pi B_G}{e^{\tilde{\tau}_A} - 1} \right]. \quad (\text{B9})$$

From Eq. (B9) follows that:

$$\frac{\pi B_G e^{\tilde{\tau}_A} - \frac{OLR}{2} \left[1 + e^{\tilde{\tau}_A} + \tilde{\tau}_A e^{\tilde{\tau}_A} \right]}{\left(e^{\tilde{\tau}_A} - 1 \right)^2} = 0. \quad (\text{B10})$$

From Eq. (B10), assuming $\tilde{\tau}_A > 0$ we get:

$$\pi B_G = OLR \frac{1 + \tilde{\tau}_A + e^{-\tilde{\tau}_A}}{2} = \frac{OLR}{f}. \quad (\text{B11})$$

Combining this equation with Eq. (28) we obtain the $\pi B_G = S_U$ equivalence requiring the thermal equilibrium at the ground surface. Note, that at real ground or sea surfaces the $\varepsilon_G \neq 1$ condition will result in the $S_G \neq S_A$ inequality, which is also apparent in *Fig. 2*.

References

- Chamberlain, S.A., Bailey, J.A., and Crisp, D., 2006: Mapping Martian atmospheric pressure with ground-based near infrared spectroscopy. *Publications of the Astronomical Society of Australia*, 23, 119-124.
- Collins, G.W. II., 2003: *The Fundamentals of Stellar Astrophysics. Part II. Stellar Atmospheres*. WEB edition, 306 pp.
- Committee on Radiative Forcing Effects on Climate Change, Climate Research Committee, and National Research Council, 2005: *Radiative Forcing of Climate Change: Expanding the Concept and Addressing Uncertainties*. The National Academies Press, USA.
- Eddington, A.S., 1916: On the radiative equilibrium of the stars. *Monthly Notices of the Royal Astronomical Society*, LXXVII. I, 16-35.
- ERBE, 2004: *ERBE Monthly Scanner Data Product*. NASA LRC, Langley DAAC User and Data Services. userserv@eosdis.larc.nasa.gov.
- Goody, R.M. and Yung, Y.L., 1989: *Atmospheric Radiation. Theoretical Basis*. University Press, Inc., Oxford, 392 pp.
- Hines, K.M., Bromwich, D.H., and Marshall, G.J., 2000: Artificial surface pressure trends in the NCEP-NCAR reanalysis over the southern ocean and Antarctica. *J. Climate* 13, 3490-3952.
- Inamdar, A.K. and Ramanathan, V., 1997: On monitoring the atmospheric greenhouse effect from space. *Tellus* 49B, 216-230.
- Karl, T.R., Hassol, J.S., Miller, D.C., and Murray, W.L., 2006: *Temperature Trends in the Lower Atmosphere*. U.S. Climate Change Science Program, Synthesis and Assessment Product 1.1, <http://www.climate-science.gov>.
- Kiehl, J.T. and Trenberth, K.E., 1997: Earth's annual global mean energy budget. *B. Am. Meteorol. Soc.* 78, 197-208.
- Lorenz, R.D. and McKay, C.P., 2003: A simple expression for vertical convective fluxes in planetary atmospheres. *Icarus*, 165, 407-413.
- McKay, C.P., Lorenz, R.D., and Lunine, J.I., 1999: Analytic solutions for the antigreenhouse effect: Titan and the early Earth. *Icarus*, 137, 56-61.
- Milne, A.E., 1922: Radiative equilibrium: the insolation of an atmosphere. *Monthly Notices of the Royal Astronomical Society*, XXIV, 872-896.
- Miskolczi, F.M. and Mlynczak, M.G., 2004: The greenhouse effect and the spectral decomposition of the clear-sky terrestrial radiation. *Időjárás* 108, 209-251.
- Miskolczi, F.M., Bonzagni, M., and Guzzi, R., 1990: High-resolution atmospheric radiance-transmittance code (HARTCODE). In *Meteorology and Environmental Sciences: Proc. of the Course on Physical Climatology and Meteorology for Environmental Application*. World Scientific Publishing Co. Inc., Singapore.
- National Research Council of the National Academies, 2004: *Climate Data Records from Environmental Satellites*. The National Academies Press, Washington DC.
- Peixoto, J.P. and Oort, A.H., 1992: *Physics of Climate*. American Institute of Physics, New York.
- Raval, A. and Ramanathan, V., 1989: Observational determination of the greenhouse effect. *Nature*, 342, 758-761.
- Sagan, C., 1969: On the structure of the Venusian atmosphere. *Icarus*, 10, 274-289.
- Stephens, G.L. and Greenwald, T.J., 1991: The Earth's radiation budget and its relation to atmospheric hydrology 1. observations of the clear-sky greenhouse effect. *J. Geophys. Res.* 96, 15311-15324.
- Stephens, G.L., Slingo, A., and Webb, M., 1993: On measuring the greenhouse effect of Earth. *NATO ASI Series, Vol. 19*, 395-417.
- Weaver, C.P. and Ramanathan, V., 1995: Deductions from a simple climate model: factors governing surface temperature and thermal structure. *J. Geophys. Res.* 100, 11585-11591.